Centralna Komisja

do Spraw Stopni i Tytułów

Załącznik nr 3 (English version)

do wniosku o przeprowadzenie postępowania habilitacyjnego

w dziedzinie nauk fizycznych w dyscyplinie fizyka

Research statement

1. First and last name: **Jacek Pniewski**

2. Diplomas and scientific degrees, including date of award and name, location of awarding institution, and title of PhD dissertation:

a) PhD degree in scope of physics, specialty: optics, awarded by the Scientific Council of Faculty of Physics, University of Warsaw, 8th December 2003. Title of the PhD thesis: *Modelling and visualisation of scalar fields on the basis of isolines.*

b) Professional title of MSc obtained in scope of physics, specialty: Fourier optics and information processing, Faculty of Physics, University of Warsaw, 1997. Title of MSc dissertation: *Image compression using morphological subband decomposition.*

3. Information on previous and current employment in research institutions.

2003–2016: assistant professor (adjunct), Information Optics Department, Institute of Geophysics, Faculty of Physics, University of Warsaw (2005–2016 Deputy Director of Institute of Geophysics).

4. Scientific achievements as per art. 16, p. 2 law dated on 14 March 2003 on the scientific degrees and on the scientific titles and on the degrees and the tile in scope of arts (Polish: Dz. U. nr 65, poz. 595 ze zm.)

a) the title of the scientific achievement

Cycle of research papers related in scope and subject: **„Modelling of light propagation and optical properties in nano– and microstructured materials"**

b) (author/authors, title/titles of papers, year of issuing, name of publisher)

JP-1. **J. Pniewski,** T. Szoplik, "Group front evolution of Gaussian beam refracted from a right- to left-handed medium," Opt. Express **14(18),** 8232—8239 (2006).
DOI: 10.1364/OE.14.008232 (Citations: WoS: 6, Scopus: 6)
Contribution of Applicant: 75%

JP-2. P. Wróbel, **J. Pniewski,** T. J. Antosiewicz, T. Szoplik, "Focusing radially polarized light by a concentrically corrugated silver film without a hole," (2009) Physical Review Letters **102(18),** 183902.
DOI: 10.1103/PhysRevLett.102.183902 (Citations: WoS: 50, Scopus: 55)
Contribution of Applicant: 40%

JP-3. R. Buczynski, **J. Pniewski,** D. Pysz, R. Stepien, R. Kasztelanic, I. Kujawa, A. Filipkowski, A.J. Waddie, M. R. Taghizadeh, "Dispersion management in soft glass all-solid photonic crystal fibers," (2012) Opto-electronics Review **20(3),** 207—215.
DOI: 10.2478/s11772-012-0033-y (Citations: WoS: 11, Scopus: 17)
Contribution of Applicant: 45%

JP-4. **J. Pniewski,** R. Kasztelanic, D. Pysz, R. Stępień, R. Buczyński, "Supercontinuum generation in all-solid photonic crystal fibers with a low index subwavelength inclusion in the core," (2013) Laser Physics **23(8),** 085104.
DOI: 10.1088/1054-660X/23/8/085104 (Citations: WoS: 4, Scopus: 4)
Contribution of Applicant: 44%

JP-5. G. Stępniewski, **J. Pniewski,** M. Klimczak, T. Martynkien, D. Pysz, R. Stępień, I. Kujawa, K. Borzycki, R. Buczyński, "Broadband dispersion measurement of photonic crystal fibers with nanostructured core," (2015) Optical and Quantum Electronics **47(3),** 807—814.
DOI: 10.1007/s11082-014-9979-y (Citations: WoS: 1, Scopus: 1)
Contribution of Applicant: 40%

JP-6. **J. Pniewski,** T. Stefaniuk, G. Stepniewski, D. Pysz, T. Martynkien, R. Stepien, R. Buczynski, "Limits in development of photonic crystal fibers with a subwavelength inclusion in the core," (2015) Optical Materials Express **5(10),** 2366—2376. (Distinction "Spotlight on optics.")
DOI: 10.1364/OME.5.002366 (Citations: WoS: 2, Scopus: 2)
Contribution of Applicant: 40%

JP-7. **J. Pniewski,** T. Stefaniuk, H. Le Van, V. C. Long, L. C. Van, R. Kasztelanic, G. Stępniewski, A. Ramaniuk, M. Trippenbach, R. Buczyński, "Dispersion engineering in nonlinear soft glass photonic crystal fibers infiltrated with liquids," (2016) Applied Optics **55(19),** 5033—5040.
DOI: 10.1364/AO.55.005033
Contribution of Applicant: 35%

JP-8. **J. Pniewski,** R. Kasztelanic, J. M. Nowosielski, A. Filipkowski, B. Piechal, A. J. Waddie, D. Pysz, I. Kujawa, R. Stepien, M. R. Taghizadeh, R. Buczynski, "Diffractive optics development using a modified stack-and-draw technique," (2016) Applied Optics **55(18),** 4939—4945.
DOI: 10.1364/AO.55.004939
Contribution of Applicant: 30%

JP-9. **J. Pniewski,** G. Stepniewski, R. Kasztelanic, B. Siwicki, D. Pierscinska, K. Pierscinski, D. Pysz, K. Borzycki, R. Stepien, M. Bugajski, R. Buczynski, "High numerical aperture large-core photonic crystal fiber for a broadband infrared transmission," (2016) Infrared Physics & Technology **79,** 10—16.
DOI: 10.1016/j.infrared.2016.09.002
Contribution of Applicant: 36%

c) discussion on the scientific goal of work and presentation of the obtained results, including discussion of the possible applications.

Contents

1. Introduction

The Applicant was employed at Faculty of Physics, Warsaw University, in the years of 2005–2016 as an assistant professor. In the years of 2005–2016 he also acted as the Deputy Director of Institute of Geophysics, Faculty of Physics, Warsaw University. Since 2011 he also has cooperated with Department of Glass in Institute of Electronic Materials Technology in Warsaw (ITME), where he was the leader of the research grant *"Analysis of generation and propagation of plasmon-polaritons in periodic subwavelength metal-dielectric waveguiding structures,"(in polish "Badanie generacji i propagacji plazmonów-polarytonów w periodycznych podfalowych metalowo-dielektrycznych strukturach światłowodowych")* funded by Polish National Science Centre, in the years of 2012–2014.

The Applicant's research cycle includes papers cited in the text as **[JP-1, JP-2, ..., JP-9]. The main topic of the research paper cycle presented by the Applicant is the possibility to predict by means of computer or numerical modelling the phenomena associated with propagation of light in nano– and microstructured materials and optical properties of light guiding structures that lead to design of optical devices.**

The cycle starts with the paper **[JP-1],** where local enhancement of the power flow in a group front of a transient sinusoidal Gaussian beam refracted at the boundary of right- and left-handed media was demonstrated. In the paper **[JP-2]** a phenomenon of focusing a radially polarized beam from the visible range by a silver film with no hole on the optical axis and double-sided concentric corrugations was shown, where the spot area was as small as $0.16\lambda^2$, and the focal length was close to λ.

Subsequent papers in the cycle focus on photonic crystal fibers (PCF) or structures that can be developed in the stack-and-draw process commonly used for PCF fabrication. In the paper **[JP-3]** the dispersion management capabilities in all–solid PCFs taking into account four thermally matched glasses which can be jointly processed were presented. As a result structures with broadband flat normal dispersion and ultra–flat near zero anomalous dispersion dedicated to supercontinuum (SC) generation with 1540 nm laser sources were shown. The paper **[JP-4]** discussed all-solid PCFs which allow to control dispersion and nonlinear phenomena by a low index subwavelength inclusion in the core and due to the use of soft glasses of high nonlinear coefficient. The obtained numerical results were further investigated and verified experimentally, and then published in the paper **[JP-5]**.

In the paper **[JP-6]** the problem of discrepancy between numerical fiber modelling results and the results obtained experimentally for fibers with nanoscale inclusion in the core was discussed. In this paper, using energy-dispersive X-ray spectroscopy technique a dramatic change in the inclusion profile and its composition caused by a non-uniform diffusion of chemical molecules during the stack-and-draw fiber fabrication process was shown.

Paper **[JP-7]** contains a numerical study on dispersion characteristic modification of nonlinear photonic crystal fibers infiltrated with liquids. In this work, a PCF based on the soft glass PBG-08, infiltrated with 17 different organic solvents, is proposed and numerical simulations of dispersion, mode area, attenuation, and supercontinuum generation are presented.

Papers **[JP-8]** and **[JP-9]** concentrate on design, numerical modelling and experimental verification of optical devices. A novel method for the development of diffractive optical elements (DOEs) was presented in the paper **[JP-8],** where the phase shift is introduced through a refractive index variation achieved by using different types of glass, and the diffractive elements are fabricated with the use of a modified stack-and-draw technique. It was shown numerically and experimentally that such a DOE can be used as a fiber interconnector that couples light from a small-core fiber into the several cores of a multicore fiber. In the paper **[JP-9]** a large mode area photonic crystal fiber (LMA PCF) made of the heavy metal oxide glass, dedicated for a broadband light guidance in the visible, near- and mid-infrared regions of wavelengths was presented. In this work we showed a proof-of-concept demonstration that a large core photonic crystal fiber is able to efficiently collect light directly from a mid-IR quantum cascade laser without use of additional optics and can be used for pigtailing mid-IR sources and detectors.

2. Numerical modelling

In all papers in the cycle, except **[JP-8]**, finite–difference methods based on solution of Maxwell equations on a regular grid were used to simulate propagation of light.

In the papers **[JP-1]** and **[JP-2]** the finite–difference time–domain (FDTD) method was applied. In this method the time-dependent Maxwell's equations are discretized using central-difference approximations, giving the space and time partial derivatives as a result. The finite–difference equations are solved in a leapfrog manner, where the electric field vector components in a given spatial volume are solved at a given instant in time, and then the magnetic field vector components in the same spatial volume are solved at the next instant in time. This process is repeated over and over again until the requested field behaviour is fully evolved. The method is, as a general rule, a fully vectorial method of computation [Taflove, 1980].

FDTD method is very demanding with regard to computational resources since all electromagnetic field components have to be stored for all points of the spatial volume, defined by the grid resolution. Simulation of spatial volumes of several micrometers in each direction requires tens of gigabytes of computer memory and parallel processing hardware and software. As a benefit, the method is flexible, works with dispersive and nonlinear media, can exploit set up symmetries, implements perfectly matched layers at boundaries etc. Like all simulation methods this also requires proper set up of sources, materials, boundaries, volumes and so on to achieve reliable results [Schneider, 2010].

In the paper **[JP-1]** the in-house FDTD software developed in Information Optics Department (IOD, Faculty of Physics, University of Warsaw) was used. In the paper **[JP-2]** the freeware package Meep [Meep] and in-house body-of revolution FDTD code were used.

In the papers **[JP-3…JP-7, JP-9]** the commercial mode solver by Lumerical was used [Lumerical]. This is a finite–difference eigenmode (FDE) solver that calculates the spatial profile and frequency dependence of modes solving Maxwell's equations on a cross-sectional mesh of the waveguide. As a result the mode field profiles, effective index, and loss are obtained. By sweeping the frequency it also allows to calculate mode dispersion. This method is based on the paper of Zhu and Brown [Zhu, 2002], with proprietary modifications and extensions. A crucial feature is the non-uniform meshing which makes it possible to increase the density of a mesh in the area containing small features.

In the paper **[JP-8]** a different simulation software was used to model propagation of light, LightTrans VirtualLab, which combines classical ray tracing technique with geometric and diffractive field tracing. This method is fast and effective in case of some microoptical setups.

In papers **[JP-3, JP-4, JP-7]** supercontinuum generation is modelled using the split–step Fourier method (SSFM). This method is used for the modelling of pulse propagation in optical fibers. The SSFM numerically solves a nonlinear Schrödinger equation separated into frequency and time domains. A linear step is made in the frequency domain, while a nonlinear step is made in the time domain [Dudley, 2010].

In the paper **[JP-5]** the finite element method (FEM) implemented in a commercial software was used to model the propagation of light in the optical fiber. In this method decomposition of the computational domain into triangles is used. Then, a set of partial derivative equations is solved locally using approximation to find the values of the electromagnetic field at points of the mesh. This method was used to verify results obtained earlier using FDE solver.

Literature (excluding papers of the Applicant's cycles of research publications)

[Taflove, 1980] A. Taflove, "Application of the finite-difference time-domain method to sinusoidal steady state electromagnetic penetration problems" IEEE Transactions on Electromagnetic Compatibility **22(3),** 191–202 (1980).

[Schneider, 2010] John B. Schneider, *Understanding the Finite-Difference Time-Domain Method,* www.eecs.wsu.edu/~schneidj/ufdtd, 2010.

[Meep] A. F. Oskooi, D. Roundy, M. Ibanescu, P. Bermel, J. D. Joannopoulos, and S. G. Johnson, "MEEP: A flexible free-software package for electromagnetic simulations by the FDTD method," Computer Physics Communications **181,** 687–702 (2010)

[Lumerical] Lumerical Solutions, Inc. *http://www.lumerical.com/tcad-products/mode/*

[Zhu, 2002] Z. Zhu and T. G. Brown, "Full-vectorial finite-difference analysis of microstructured optical fibers," Opt. Express **10(17),** 853–864 (2002).

[Dudley, 2010] *Supercontinuum Generation in Optical Fiber,* edited by J.M. Dudley, J.R. Taylor, Cambridge University Press, 2010.

3. Light propagation in effectively negative materials

In the years of 2004–2008 the Applicant was involved in research grants focused on metamaterials, namely "Metamaterials for radio and millimetre wavelengths and photonic superlattices engineering" (in polish "Metamateriały dla fal radiowych i milimetrowych oraz inżynieria fotonicznych supersieci"), "Metamaterial made of dielectrics and nanowire lattices: design, development and characterisation" (in polish "Metamateriał z dielektryka i sieci nanodrutów: projektowanie, wytwarzanie i charakteryzacja"). The Applicant also participated in the 6th EU Framework Program: Network of Excellence: Metamaterials Organised for radio, millimeter wave and Photonic Superlattice Engineering (Metamorphose) and was a member of Scientific Committee in the EU COST Action P11: *Physics of linear, non-linear and active photonic crystals, 2003–2007,* and participated in EU COST Action 288: *Nanoscale and ultrafast photonics.*

The concept of metamaterials that are materials with unusual electromagnetic properties was extensively investigated at that time. There are many definitions of metamaterials, which highlight various aspects of this concept. One of the most flexible definition states that "Metamaterial is an arrangement of artificial structural elements, designed to achieve advantageous and unusual electromagnetic properties." The concept of material denotes homogeneity, and, if a metamaterial is a periodical structure, the lattice constants should be considerably smaller than the wavelength used.

Starting from the theoretical work by Veselago [Veselago, 1968] it was expected that refraction of a wavefront of a continuous wave or pulse at a metamaterial interface should be negative in some situations [Smith, 2000; Ziolkowski, 2001; Gupta, 2004], when an electromagnetic wave incidents at the interface between a nondispersive right–handed material (RHM) and a strongly dispersive lossy left–handed medium (LHM). To that time observations of unusual behaviour of continuous wave (CW) Gaussian beams on a boundary between RHM and LHM addressed refraction and retardation effects and focusing with double negative (DNG) slabs. **In the paper [JP-1] the Applicant and his collaborator prof. Tomasz Szoplik have shown that wave front of CW Gaussian beam that incidents normally on the interface undergoes local enhancement of the power flow and shape modification of envelope of amplitudes of a group of interfering waves with different frequencies.** In the FDTD simulation CW Gaussian beam of wavelength $\lambda = 500$ nm was generated in an empty 2D half-space and incident at the interface between vacuum and a DNG material. The metamaterial electric permittivity $\varepsilon(\omega)$ and magnetic permeability $\mu(\omega)$ were described by lossy Drude model, with equal electric and magnetic plasma frequencies $\omega_{pe} = \omega_{pm} = \omega_p = 5.96 \times 10^{15}$ rad/s for the frequency $f_0 = 600$ THz and $n = -1.5$. Figure 1 shows propagation of CW Gaussian beam through an interface between vacuum with $n = 1$ and lossy $n = -1.5$ medium.

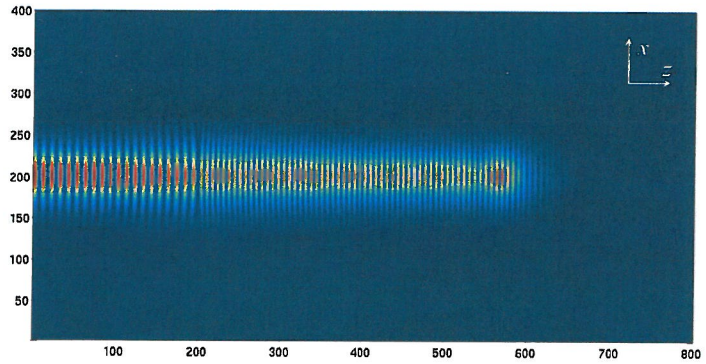

Fig. 1. CW Gaussian beam incidents normally at the interface ($z = 200$) between vacuum and LHM with $n = -1.5$. Evolution of the absolute value of Poynting vector $|\mathbf{E}\times\mathbf{H}|$, where $\mathbf{H}$ is parallel to the image plane, is shown in pseudocolors normalized to the maximum value in the incident beam.

Figure 2 shows CW Gaussian beam of wavelength $\lambda = 500$ nm that incidents at the interface at 45° angle. In the case of oblique incidence of CW Gaussian beam at RHM-LHM interface we observe the following three effects. Firstly, the negative refraction into DNG medium with $n = -1.5$ reported before in several papers. Antiparallel group and phase velocities shown with red and blue vectors, respectively, are perpendicular to phase fronts denser than in vacuum. The direction of energy transport is parallel to the group velocity and normal to phase fronts. Secondly, modulation interference fronts that is group fronts move sideways with respect to the propagation direction of phase fronts as it was first observed by Smith et al. [Smith, 2002]. **We, for the first time, showed the third effect of transient amplitude enhancement of the envelope of positively refracted group fronts of CW Gaussian beam.** This purely dispersion effect results from different angles of refraction and diversified phase speeds of

individual Fourier components of the Gaussian beam in LHM with $n = -1.5$. The group front build-up develops during about 50 wave periods behind the interface and propagates along several wavelengths.

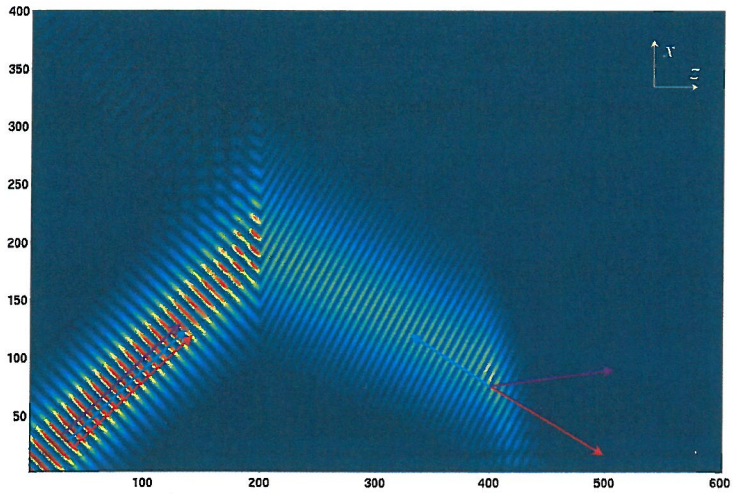

Fig. 2. CW Gaussian beam incidents at 45° at the interface ($z = 200$) between vacuum and DNG medium with $n = -1.5$. Pseudocolored evolution of the absolute value of Poynting vector $|\mathbf{E}\times\mathbf{H}|$, where $\mathbf{H}$ lays in the figure plane, is normalized to maximum value in the incident beam. In incident and refracted beams red, violet and blue vectors indicate group, group front, and phase velocities, respectively.

Literature (excluding papers of the Applicant's cycle of research publications)

[Veselago, 1968] V. G. Veselago, "The electrodynamics of substances with simultaneously negative values of ε and μ," Sov. Phys. Usp. **10,** 509—514 (1968).

[Smith, 2000] D. R. Smith and N. Kroll, "Negative refractive index in left-handed materials," Phys. Rev. Lett. **85,** 4184—4187 (2000).

[Ziolkowski, 2001] R. W. Ziolkowski and E. Heyman, "Wave propagation in media having negative permittivity and permeability," Phys. Rev. E **64,** 056625-1-15 (2001).

[Gupta, 2004] S. Dutta Gupta, R. Arun and G. S. Agarval, "Subluminal and superluminal propagation in a left-handed medium," Phys. Rev. B **69,** 113104-1-4 (2004).

[Smith, 2002] D. R. Smith, D. Schurig, and J. B. Pendry, "Negative refraction of modulated electromagnetic waves," Appl. Phys. Lett. **81,** 2713—2715 (2002).

4. Enhanced transmission of light through subwavelength structures in metal nanolayers

The scientific interest of the Applicant moved to plasmonics in the years of 2008–2012. At that time he was a contractor in the research grants *"Nanooptical superlens made from metamaterial in the photonic connector" (in polish "Nanooptyczna supersoczewka z metamateriału w złączu fotonicznym")* and *"Plasmonic Superprism" (in polish "Superpryzmat plazmoniczny").* He also participated in EU COST Action MP0702: *Towards Functional Sub-Wavelength Photonic Structures, 2008–2012.*

As a result of this interest several papers, including conference proceedings, were published, co-authored by the members of Information Optics Department at Faculty of Physics, Warsaw University (P. Wróbel, T. Szoplik, T.J. Antosiewicz, W.M. Saj) and papers resulting from collaboration with scientists from Institute of Condensed Matter Theory and Solid State Optics, Friedrich-Schiller-Universität Jena (C. Rockstuhl, S. Mühlig) and Department of Radio Science and Engineering/SMARAD, Helsinki University of Technology (C.R. Simovski, S.A. Tretyakov).

Plasmonics is the study and application of the interactions of optical-frequency electromagnetic field oscillations with the free electrons in a metal. These electrons behave like a charge-separated gas, and can be called plasma. Key advantage of plasmonic devices is that they allow to confine electromagnetic

oscillations at optical frequencies to volumes that could be smaller than the wavelength that would be generated in free space at that frequency. It is also possible to create extremely intense, concentrated electromagnetic fields, useful in such applications as single-molecule spectroscopy (e.g. SERS, Surface-Enhanced Raman Spectroscopy).

One of the interesting phenomena is enhanced transmission of light through subwavelength holes in metal nanolayers that originates from a paper of Ebbesen et al. [Ebbesen, 1998]. Enhancement means that the amount of transmitted light related to that of impinging onto the holes exceeds unity. The intensity of transmitted light increases even more when a single aperture of diameter $a << \lambda$ is surrounded by a set of concentric, periodic, and subwavelength corrugations which permit excitation of surface plasmon-polaritons (SPPs).

In the paper [JP-2] a phenomenon of focusing a radially polarized Laguerre-Gauss beam from the visible range by a silver film with no hole on the optical axis and double-sided concentric corrugations was shown for the first time, based on FDTD simulations. In this way a nanolens that focuses the beam into spot of full width at half maximum equal to about 0.46λ was proposed. At $\lambda = 500$ nm this plasmonic lens has a focal length equal to λ and acts as a high numerical aperture (NA) refractive optical system of NA = 0.98. At $\lambda = 400$ nm the focal length is 2λ and NA = 0.92. In Fig. 3 the schematic of the lens is shown. In Fig. 4 the normalized electric energy density distribution in the vicinity of the nanolens is presented.

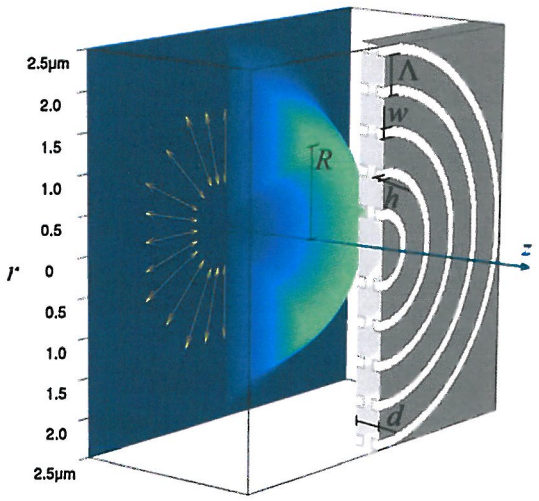

Fig. 3. Light beam with Laguerre-Gauss intensity profile and pure radial polarization indicated by yellow arrows illuminates an apertureless silver film of a thickness d = 100 nm along the z axis. The depth and the width of periodic corrugations with lattice constant Λ = 500 nm are equal h = 40 nm and w = 100 nm, respectively. The radius of the maximum intensity of the beam is R.

Focusing of radially polarized light into a tight spot results from two independent factors. The first is highly efficient photon-to-plasmon coupling which is possible due to almost 100% radial polarization achievable also in experiment [Quabis, 2005]. Thus, the amount of light with linear or azimuthal polarization is negligible and there is virtually no background emission that decreases the signal-to-noise ratio in the focal region. The second is connected with evolution of radial and longitudinal components of transmitted electric field behind the lens. The radial components of E field on subsequent corrugations is in phase and propagates as higher order radially polarized beams. The longitudinal components of E field influence convergence of transmitted beam. The radial components of E field interfere destructively on the axis, while the longitudinal component of E field is especially reinforced due to constructive interference. In the focal region the energy is transferred from the radially polarized electric field components to longitudinally polarized ones and the longitudinal component of E field is

about 10 times stronger than incident onto the structure. Reinforcement of the axial component depends on the number of illuminated grooves and range of plasmons. The study was further investigated by the same authors in the paper [Wróbel, 2011]. **Such a lens could be used in micro– and nanooptics, for example as light coupling device.**

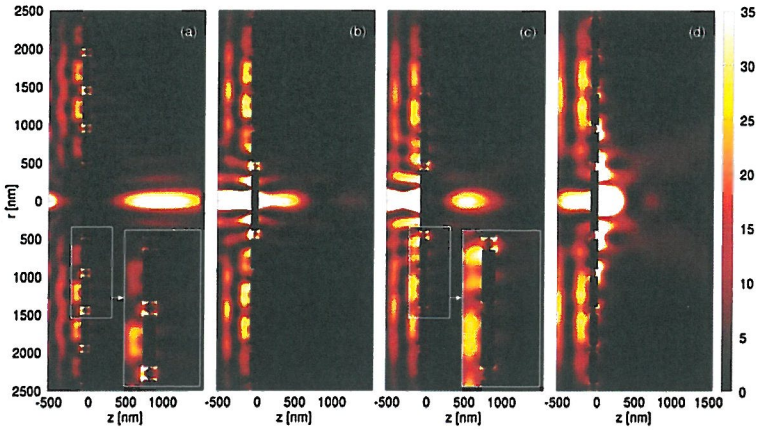

Fig. 4. Normalized electric energy density $|E|^2$ distribution in the vicinity of the nanolens for R = 1400 nm for wavelengths (a) 410 nm, (b) 460 nm, (c) 500 nm, and (d) 600 nm.

Literature (excluding papers of the Applicant's cycle of research publications)

[Ebbesen, 1998] T.W. Ebbesen, H.J. Lezec, H.F. Ghaemi, T. Thio, P.A. Wolff, "Extraordinary optical transmission through sub-wavelenght hole arrays," Nature **391 (6668),** 667—669 (1998).

[Quabis, 2005] S. Quabis, R. Dorn, G. Leuchs, "Generation of a radially polarized doughnut mode of high quality," Applied Physics B **81(5),** 597-600 (2005).

[Wróbel, 2011] P. Wróbel, T. J. Antosiewicz, J. Pniewski, T. Szoplik, "Single-layer metal nanolenses with tight foci in far-field,"Applied Physics A: Materials Science and Processing **103(3),** 821—825 (2011).

5. Optical phenomena and properties of photonic crystal fibers

In the years of 2009–2016 the Applicant joined a work group led by Ryszard Buczyński (University of Warsaw/Institute of Electronic Materials Technology/Heriot-Watt University). The Applicant was a contractor in the Polish National Science Centre research grant *"Photonics fibers for supercontinuum generation in the mid infra red" (in polish "Włókna fotoniczne do generacji supercontinuum w zakresie średniej podczerwieni")* in the years of 2010–2012. He was also the leader of the Polish National Science Centre research grant *"Analysis of generation and propagation of plasmon-polaritons in periodic sub-wavelength metal-dielectric waveguiding structures" (in polish "Badanie generacji i propagacji plazmonów-polarytonów w periodycznych podfalowych metalowo-dielektrycznych strukturach światłowodowych")* in the years of 2012–2014. One of the result of this grant was an international patent application *„ A photonic crystal fibre for transferring radially polarised light beam and a method of manufacturing such a fibre" (in polish "Światłowód fotoniczny do przenoszenia wiązki światła spolaryzowanej radialnie i sposób wytwarzania takiego światłowodu").*

The collaboration within the work group resulted in several papers, including **[JP-3...JP7],** where various aspects of PCFs made of soft glasses were investigated numerically and experimentally.

In the paper [JP-3] dispersion management capabilities and supercontinuum generation in all–solid photonic crystal fibers made of soft glasses were demonstrated. The tailoring of the group velocity dispersion (GVD) of an optical fiber was and still is critical to the successful utilization of nonlinear optical properties in applications such as supercontinuum generation, harmonic generation and wavelength conversion via stimulated Raman scattering. One of the optical structures that can be

used to tailor the GVD is holey or photonic crystal fiber (PCF), e.g., a microstructured fiber with longitudinal holes in the cross–section. Due to the high refractive index contrast between glass and air, along with freedom of choice of the holes' geometrical parameters, one can precisely control dispersion behaviour and nonlinearity of the fibers [Bartelt, 2007]. However, this approach has serious technological drawbacks resulting in unintended distortions of the lateral profile that influence the dispersion properties of the fibers [Buczyński, 2011].

For PCF development soft glasses can be used. In this way, one can combine the unique properties of that class of glasses, such as high nonlinearity, gain and transmission in the near infrared with the wave guiding properties of PCFs, namely single mode guidance for large mode areas and tight mode confinement.

In our research we decided to use all–solid photonic crystal fibers (APCFs), which are an alternative to air–glass solid core PCFs. In ACPFs, the air holes are replaced with glass microrods of a refractive index different from that of the background glass. Index guiding and photonic bandgap guiding mechanisms can exist in APCFs depending on the refractive index of the core. The development of the first all–solid PCF with a high index core was reported by Feng at al. [Feng, 2003] The advantages of all–solid PCFs, as compared to the air–hole based PCFs, are relatively simple fabrication and a possibility to glue or splice nonlinear fibers with standard optical fibers. Moreover, the fiber parameters' control during the drawing process is much simpler and the development of parameters similar to the designed ones is straightforward. In addition, the APCFs have unique spectral and dispersion properties that are suitable for applications in low–loss fiber lasers, nonlinear optics, birefringent fibers.

In the paper [JP-3], a special APCF, made from soft glasses: SF6/LLF1, SF6/F2, and F2/NC21 was proposed, analysed numerically, and then developed, for the first time. The glasses SF6, LLF1, and F2 are commercially available glasses from Schott. The glass NC21 was developed at Institute of Electronic Materials Technology to replace LLF1 glass, which exhibit tendency for crystallisation. The new glass has superior rheological properties to the commonly used LLF1 glass. Mentioned pairs of thermally matched glasses are selected and analysed numerically. Each pair consists of a glass with a high refractive index as a host material and a glass with a low refractive index. The core is always made of F2 or SF6 glass.

The schematic of an APCF is shown in Fig. 5. A fiber consists of inclusions of a low refractive index material that are embedded in a host material of a higher refractive index where the single central microrod is omitted. Therefore, the core has a higher refractive index than the cladding and the effective index guidance is a dominant mechanism in this case. We studied the influence of the fiber structure on the dispersion in terms of lattice constant Λ, filling factor f and glass selection. The glass selection determines the wavelength dependent refractive index difference Δn and dispersion properties of the fiber. In Fig. 6 the refractive indices and the dispersion of the glasses are presented with reference data of pure silica glass. It is clear that the NC21 glass is relatively similar to the LLF1 glass in terms of material dispersion and refractive index. The zero dispersion wavelength (ZDW) for the NC21 glass is located 50 nm away from the ZDW for LLF1 glass.

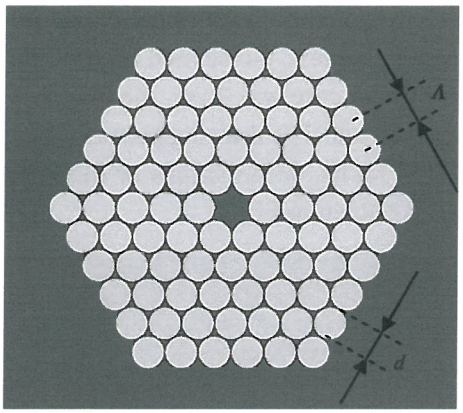

Fig. 5. Geometry of analysed all–solid photonic crystal fiber. Filling factor f is defined as d/Λ.

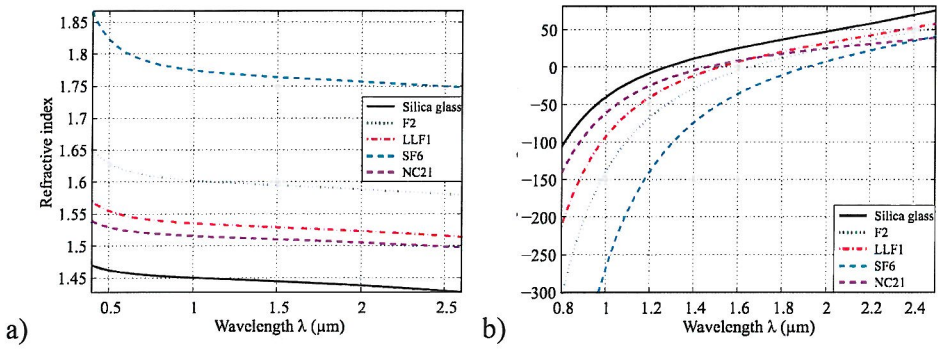

Fig. 6. (a) Refractive index, and (b) dispersion of bulky soft glasses NC21, LLF1, SF6 and F2. As a reference data of the pure silica glass is shown.

Numerical simulations were conducted to analyse dispersion control ability as a function of material choice and geometrical parameters of the cross–section profile. For example, **it was shown that for SF6/LLF1 fiber zero dispersion wavelength shift is possible along with near zero ultra flat anomalous dispersion below 5 ps/nm/km over 300 nm** for a fiber structure: lattice constant Λ = 1.8 μm and d = 1.7 μm (see Fig. 7).

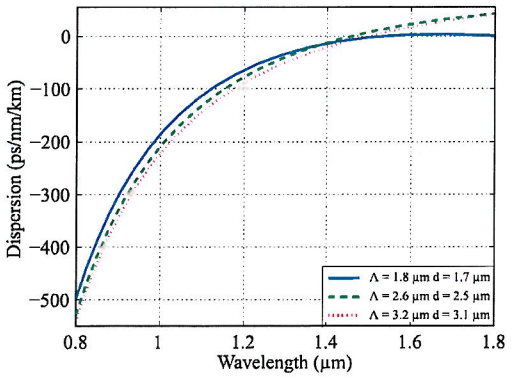

Fig. 7. Dispersion properties of photonic crystal fiber made of SF6/LLF1 glasses as a function of lattice constant with high filling factor above 0.94.

A selected pair of glasses F2/NC21 was then chosen to develop a fiber with the refraction index contrast of Δn = 0.1. On the basis of the numerical simulations, the following geometrical parameters of the structure were selected: lattice constant Λ = 1.8 μm, filling factor $f = d/\Lambda \geq 0.9$. A hexagonal structure with the core made of F2 glass, containing 15 elements on the diagonal, was prepared. The basic element

of the structure is in the shape of a hexagon built from an NC21 rod (lower refractive index) surrounded by a single ring made from F2 glass to achieve the desired high filling factor. The external diameter of the fiber was 123 μm, the diameter of the core was 2 μm, the diagonal of the photonic structure was 31 μm and the lattice constant was $\Lambda = 2.1$ μm. The drawing process was very stable and the final fiber has a high quality regular structure – no faults, deformations or other defects were observed. The cross-section of the APCF (SEM image) is shown in Fig. 8.

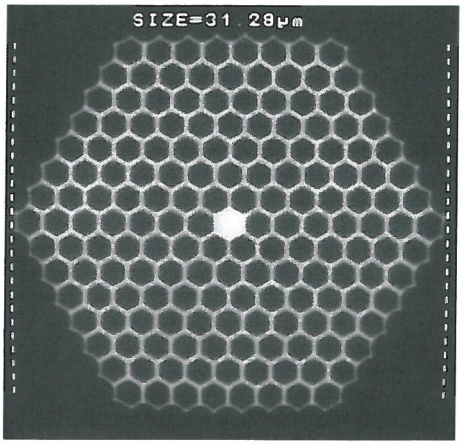

Fig. 8. Cross–section of developed all–solid photonic crystal fiber made of F2/NC21 glasses.

The effective refractive index and the dispersion of the developed fiber were numerically simulated using the SEM image. The effective refractive index of the fundamental mode was equal to $n_{eff} = 1.5953$ at 800 nm while the effective mode area was 4.3 μm^2. The birefringence of the fiber was lower than 0.3 × 10^{-5}. Calculated dispersion characteristics show normal dispersion between 0.8–1.8 μm (see Fig. 9).

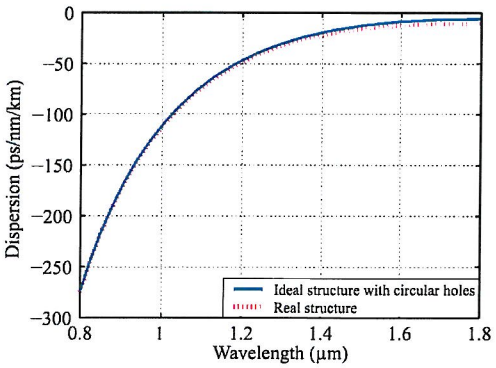

Fig. 9. Calculated dispersion characteristics based on developed APCF with F2/NC21 glasses.

We have measured the attenuation of a 2.5 m long sample of the fiber using the standard cut–back technique. As a source we used a 825 nm superluminescent diode with a 30 nm FWHM spectrum. The measured attenuation of the fiber is below 7.5 dB/m.

The obtained dispersion characteristics shows that the developed fiber is well optimized for supercontinuum generation in the normal dispersion regime with a source that emits at 1540 nm. However, preliminary tests were performed using a Ti:Sapphire femtosecond oscillator working at the wavelength of 792 nm. We have also calculated numerically broadening effect for 800, 1500 and 1600 nm. Sample results are plotted in Fig. 10.

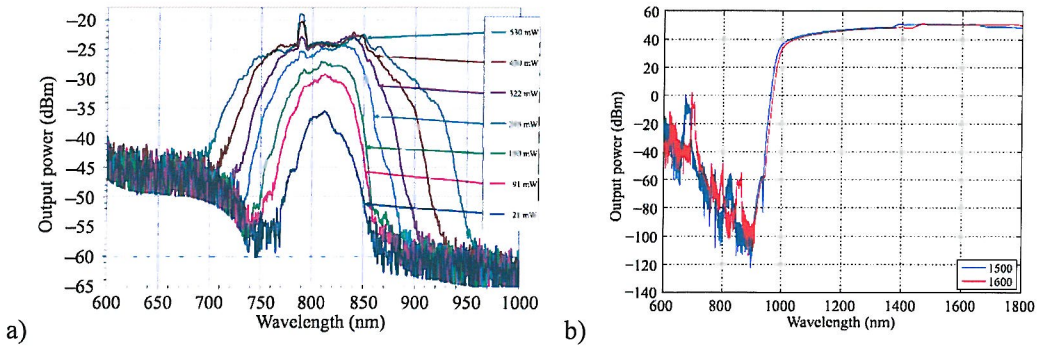

Fig. 10. Numerical simulations of supercontinuum generation in developed fiber a) a function of pumping power. b) as a function of pumping pulse wavelength, 1500 nm and 1600 nm.

As a result of the paper [JP-3] we were able to design and simulate numerically APCFS, dedicated to SC generation, made from soft glasses, and then develop selected modelled APCFs in the stack-and-draw process.

The APCFs were further investigated in the paper **[JP-4]**. In this paper dispersion management and SC generation capabilities in APCFs with a low index subwavelength inclusion in the core were presented. The inclusion makes it possible to engineer the dispersion profile while maintaining a constant effective mode area. The geometry of this fiber is shown in Fig. 11.

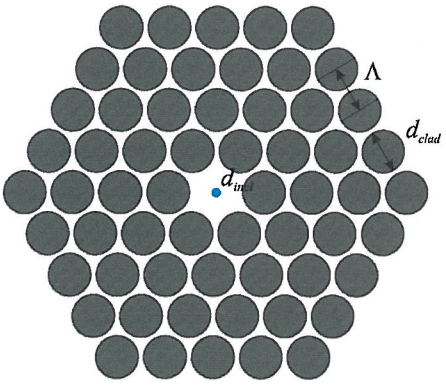

Fig. 11. The basic geometry of the analyzed APCF.

Prior to publication of our paper, several authors discussed the possibility of SC generation in APCFs using soft glasses or with different geometries of the core [Argyros, 2005; Camerlingo, 2010; Ghosh, 2010]. Highly nonlinear PCFs have been used successfully for broadband supercontinuum generation with low intensity input pulses [Domachuk, 2008]. However, the zero dispersion wavelength (ZDW) of these bulky glasses remained in the infrared region. As a result, the dispersion properties of the classical small-core PCFs prevented the use of highly efficient and low cost nanosecond lasers as pump sources. Moreover, popular highly nonlinear soft glasses, such as LLF1, SF6 and SF57 are not well–suited to cheap stack-and-draw technology because of their high crystallization behaviour, and are reserved for fiber development with the use of extrusion processes.

As it was shown in the paper **[JP-3]** the development of APCFs in the stack-and-draw process allows the precise control of all the parameters of the developed fiber in very good agreement with the design criteria. For example, the shift of the ZDW of the fundamental mode can be achieved through reduction of the solid core diameter. However, the freedom of engineering the group velocity dispersion (GVD)

is usually very limited, and the tailoring of the GVD of an optical fiber is critical to the successful utilization of nonlinear optical properties in applications such as supercontinuum generation, harmonic generation and wavelength conversion via stimulated Raman scattering. With the reduction of the core diameter, the effective modal area decreases. This results in an increase of the nonlinear coefficient of the fiber and the reduction of the coupling efficiency for the pump beam. An alternative method of tailoring the dispersion properties of a PCF is structuring of the core. This method gives more freedom in dispersion tailoring.

In the paper [JP-4], for the first time, we reported on dispersion management and supercontinuum generation capabilities in high-contrast APCFs made of soft glasses (SF6/NC21) with a low index subwavelength inclusion in the core. The inclusions make it possible to engineer the dispersion characteristic while maintaining a constant effective mode area.

The proposed fiber consists of inclusions of a low refractive index material (in–house developed NC21 glass), embedded in a host glass (Schott SF6) of higher refractive index, where a single central microrod is omitted to create the core of the fiber. Both glasses are thermally matched and can be jointly processed in a fiber drawing process. In addition, a nano-inclusion of NC21 glass is located centrally in the core. For modelling, we considered the diameters of cladding inclusions in the range of 1.425–4.75 μm, while the lattice constant for the cladding was in the range of 1.5–5 μm. The nano-inclusion in the core had a diameter ranging from 100 to 500 nm. The average refractive index of the core was higher than that of the cladding and the effective index guidance was the dominant guiding mechanism. The filling factor of the cladding was equal 0.95. An example of dispersion and mode area engineering is shown in Fig. 12 and in Table 1.

We decided also to develop an APCF fiber with a 200-nm nano-inclusion in the core. The high filling factor of the cladding leads to a large number of propagating high order modes in the first design. To suppress them, the structure of both modelled and developed APCFs was refined in such a way that for the first ring of rods the filling factor is 0.95 and for the other rings equals 0.4. For the development, a hexagonal structure containing 13 elements on the diagonal was prepared as a preform. The intended lattice constant was equal to 1.8 μm and the diameter of the nano-inclusion in the core was 300 nm.

Three fibers, labeled NL26A 1, NL26A 2 and NL26A 3, were drawn with different sizes of photonic cladding, that is 32,12 μm; 27,00 μm and 22,36 μm, respectively. The drawing process was very stable and the final fiber had a high quality regular structure. In Fig. 13 SEM images of the cross-section of the developed fiber NL26A 3 are shown.

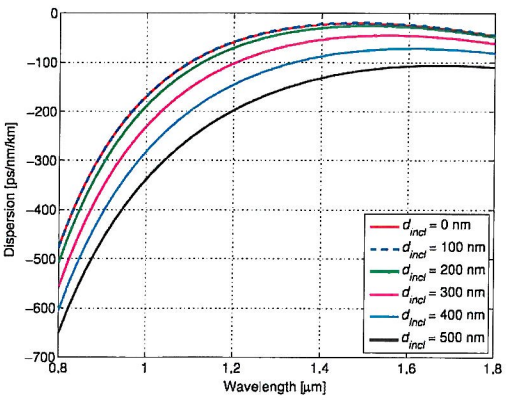

Fig. 12. Calculated dispersion of the APCF made of SF6/NC21 glass as a function of the diameter of the nano-inclusion in the core and for the lattice constant Λ = 1.5 μm.

Table 1. Calculated effective mode areas of the fundamental mode for the analysed cross-sections.

Diameter of the inclusion [nm]	Fundamental mode area [μm²]
0	1.496
100	1.522
200	1.568
300	1.729
400	2.009
500	2.081

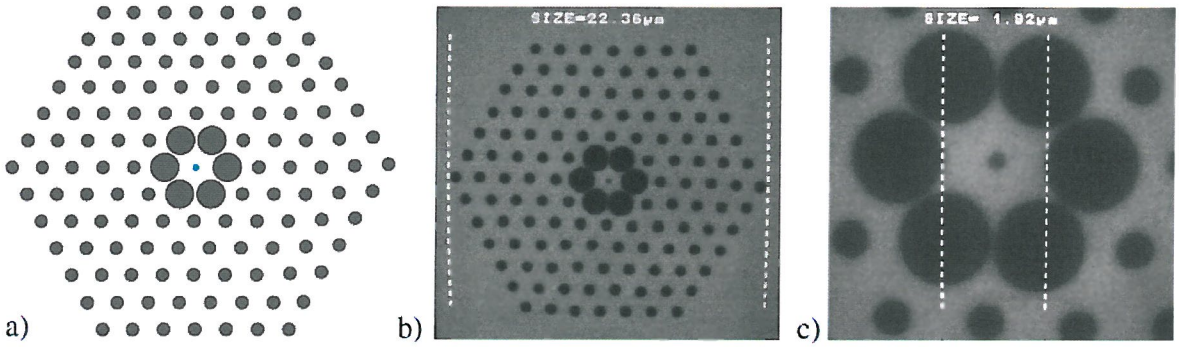

Fig. 13. (a) Schematic of the fiber structure. (b) SEM image of the cross-section of the developed fiber NL26A 3. (c) SEM image of the cross-section of the core area of the developed fiber NL26A 3.

On the basis of SEM images, the dispersion was calculated numerically. The dispersion characteristics of the developed fiber NL26A 3 are shown in Fig. 14. Although the size of the developed nano-inclusion in the core in the SEM image is identified as 300 nm, the dispersion profile is very close to the theoretical results for the core inclusion of 200 nm. The difference is mainly caused by glass diffusion at glass boundaries. Moreover, numerical modelling of the dispersion profile uses a step-like refraction index, while the mixing of glasses leads to a continuous profile of the refraction index and a smaller effective diameter of the nano-inclusion. This issue was later addressed in the paper **[JP-6]**.

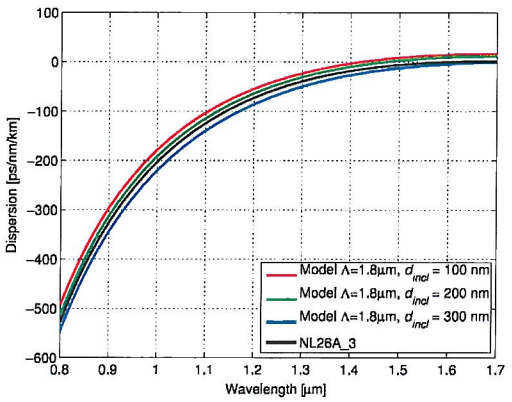

Fig. 14. Comparison of calculated dispersion profiles based on a SEM image of developed fiber NL26A 3 with theoretical models having different diameters of the nano-inclusion in the core.

Dispersion characteristics calculated for the developed fiber NL26A 3 were used to simulate SC generation using the split-step Fourier method. In the simulation we assumed a source wavelength of 1550 nm and a maximum fiber length of 0.3 m. The pulse duration equals 100 fs, and the pulse energy ranges from 3 to 12 nJ. The attenuation of the fiber was not taken into account, since only very short

fragments of fiber (of a few centimeters) were used. It was supposed that in this case attenuation did not significantly influence the output characteristics of the supercontinuum. The remaining parameters significant for the simulation are discussed in the publication. The simulations were limited to the range of 800–2000 nm since we focused only on an ultraflat supercontinuum with intensity fluctuation below 3 dB. The density plot of the spectral evolution of supercontinua and spectral characteristics are shown in Fig. 15. **The proposed fiber with ultraflat broadband characteristics of a supercontinuum is a candidate for a new efficient light source for optical coherent tomography and multiple band telecommunication applications.**

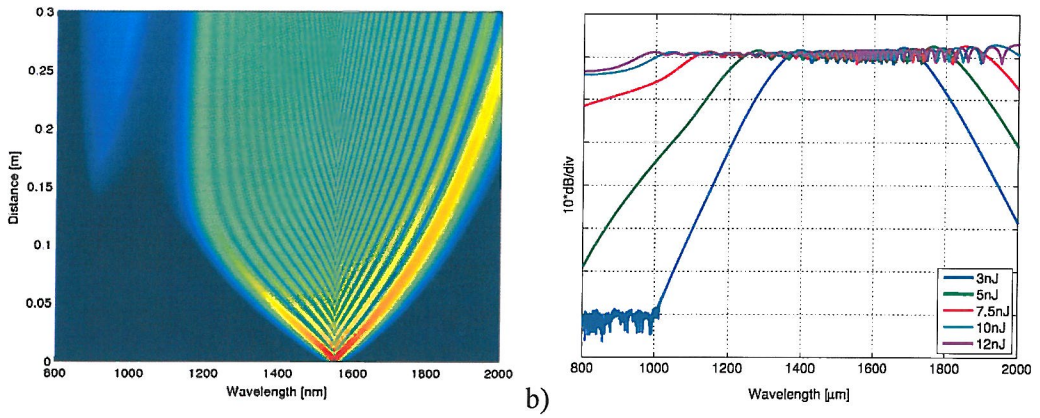

Fig. 15. a) Density plots of the spectral evolution of SC generated with pulses of wavelength of 1550 nm and energy of 3 nJ. b) Spectral characteristics for the SC generated with pulses of different energy for the developed fiber NL26. The attenuation is calculated for the 5-cm-long fiber.

As a result of the paper APCFs with a low index subwavelength inclusion in the core that allow the engineering of the fiber dispersion profile while maintaining a small mode field area, made of soft glasses, were introduced.

Apart from scientific publications the Applicant's research in the field of APCFs presented in **[JP-4]** resulted in an international patent application "A photonic crystal fibre for transferring radially polarised light beam and a method of manufacturing such a fibre " co-authored by R. Buczyński, T. Stefaniuk, J. Pniewski, D. Pysz, G. Stępniewski, R. Stępień.

In the paper **[JP-5]** the Applicant continued the research on the APCFs with a nano-inclusion in the core, shown earlier in Fig. 13. This research was focused on the reliability of dispersion measurement in APCFs, which are usually developed in short sections. The SC generation phenomena rely directly on the dispersion characteristic, thus, the proper modelling, characterisation and verification of the simulation results are crucial for SC. Widely used techniques for dispersion characterisation, like the time-of-flight method or the modulation phase shift method [Cohen, 1985], require use of long sections of optical fibers. Apart from high cost, mentioned techniques are inapplicable for optical fibers made of highly nonlinear glasses due to their high attenuation. Another approach is to use an interferometer combined with a broadband light source [Didams, 1996]. A modified Mach–Zehnder interferometer technique enables reliable measurement of dispersion characteristic in short lengths of optical fiber [Hlubina, 2007]. **We used this relatively cheap and easily applicable method for dispersion measurements of all-solid microstuctured fiber with nano-inclusion in the core. We obtained results of measurements for the APCF made of soft glasses SF6/NC21, for the first time.**

First, we measured the attenuation of the fiber using the standard cut–back method. Measured loss for wavelength 780 nm reaches 20 dB/m and is caused mainly by material losses, which are typically several dB/m for heavy metal oxide silicate glasses, and of waveguide losses typical for small core fibers. Due

to high attenuation the relatively short sample of the fiber with the length of 65.20 mm was measured in the Mach–Zehnder interferometer, shown in Fig. 16. The detailed description of the experimental setup is discussed in the paper [JP-5].

In Fig. 17 measured relative group index as a function of wavelength is shown, compared to the numerical simulations on the basis of SEM image of the fiber and the material dispersion of the glasses.

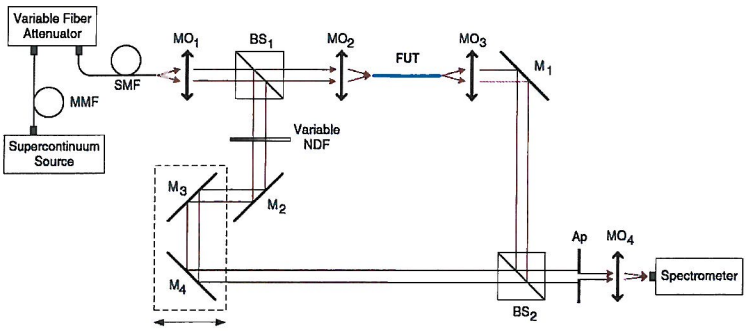

Fig. 16. Unbalanced Mach–Zehnder interferometer setup used for dispersion measurement.

Due to discrepancy between dispersion characteristics modelled in the paper [JP-4] and obtained experimentally, we verified the dispersion profiles with finite element method (FEM), and got the same results as with FDTD method. We assigned the differences to several effects. First, we assumed sharp transition between SF6 and NC21 glasses in numerical simulations. However, diffusion occurs between glasses and transition between glasses is smoothed in a real fiber structure. Second source of error introduced into the simulation is uncertainty of geometric dimension reading from the SEM images. In addition, calculations introduce errors with limited mesh size and assumed material dispersion characteristics. As a result, developed fiber has ZDW shifted by 164 nm toward longer wavelengths with respect to design and cannot be used for efficient supercontinuum generation with 1550 nm femtosecond fiber lasers as pump source as it was predicted in the paper [JP-4]. For this purpose, further optimization of fiber design and fiber drawing is required. The dispersion curve can be lifted up and the ZDW can be pushed into the shorter wavelengths in a new fiber with larger pitch and with larger inclusion in the core. The developed fiber can be considered for SC generation in anomalous dispersion range with thulium femtosecond lasers which operate around 2 μm.

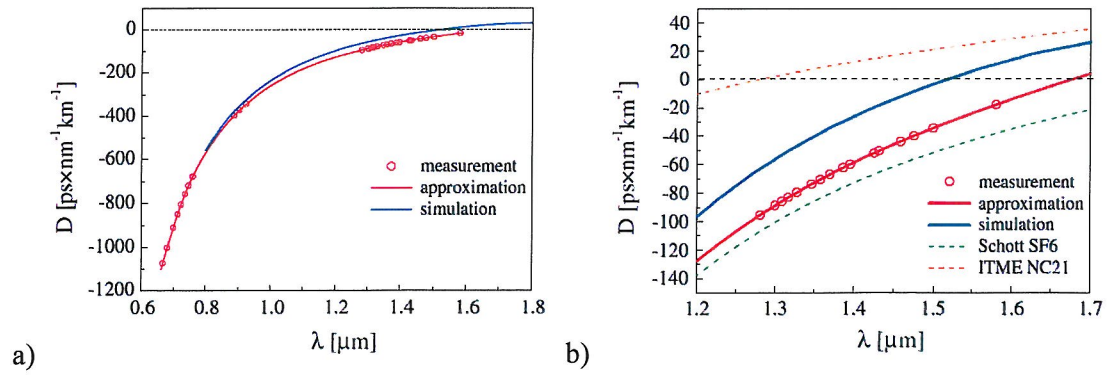

Fig. 17. a) Calculated and measured fiber dispersion—an overview. b) Calculated and measured fiber dispersion in proximity of zero dispersion wavelength. Blue solid line on the dispersion characteristic shows numerically obtained dispersion of the fiber. Dash lines show material dispersion of the bulk glasses.

In the paper [JP-6] the problem of discrepancy between numerically modelled and experimentally measured dispersion characteristics was deeply investigated for a PCF with a subwavelength nano-

inclusion in the core, shown schematically in Fig. 11. This issue was indicated in the previous papers **[JP-4]** and **[JP-5]**. Prior to publication of the paper there was an interest in structuring the core of PCFs, for example to influence nonlinearity of the fiber [Biancalana, 2010], for spectral tunneling of solitons [Kibler, 2007] and for the enhancement of cylindrical birefringence [Euser, 2011]. The concept of a fiber for mid-IR with a microporous PCF based on chalcogenide glasses was introduced and modelled by Ung and Skorobogatiy [Ung, 2010]. PCFs with an inclusion in the core based on soft glasses were developed and shown to enable the generation of supercontinuum [Buczyński, 2011].

In the paper we have considered a previously developed PCF with a high refractive index inclusion in the core. The fiber is made of NC21 silicate glass. The inclusion was made of Schott lead silicate SF6 glass.

For a PCF without an inclusion in the core only the fundamental mode can be excited effectively, assuming a linearly-polarized Gaussian beam at the wavelength of 800 nm. This mode has the mode area of 2.12 μm^2. We expected that the embedment of an inclusion which has a higher refractive index than that of the background glass in the core decreases the fundamental mode area, which in turn leads to an increase of the nonlinear coefficient of the fundamental mode. The fundamental mode area as a function of the diameter of the inclusion is shown in Fig. 18. For the inclusion diameter in the range of 400–680 nm, the mode area remains lower than 0.4 μm^2 for the wavelength of 800 nm, which allows to obtain a desirable high energy density. At the same time the mode area of higher order modes is similar to the case when the core does not have any inclusion. This allows to spatially separate different optical modes supported by the fiber.

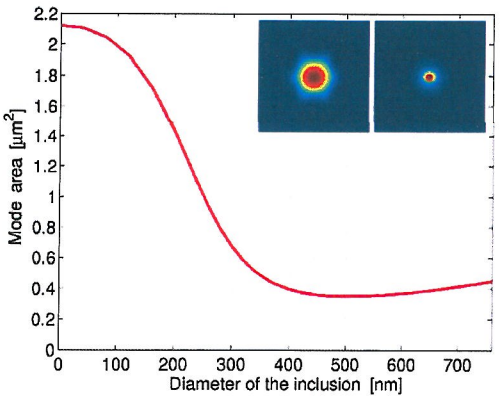

Fig. 18 The fundamental mode area as a function of the diameter of the inclusion for the numerically modelled fiber and the wavelength equal to 800 nm; In the inset, the relative intensity of the maximum (no inclusion) and minimum (inclusion diameter of 500 nm) fundamental mode area is shown.

The ZDW of the fundamental mode is highly sensitive to parameters of the inclusion, especially to the diameter and the material dispersion characteristic of the glass used. It is shifted approximately 1.8 μm towards longer wavelengths when the diameter of the inclusion changes from 0 (no inclusion) to 800 nm, as shown in Fig. 19.

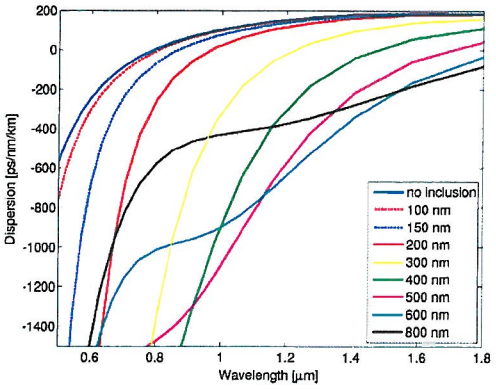

Fig. 19. Dispersion characteristics of photonic crystal fibers with the hexagonal lattice constant $\Lambda = 1.8$ μm and the relative air-hole size $d/\Lambda = 0.91$ with a high refractive index subwavelength inclusion in the core of the diameter in the range of 0–800 nm.

For the ideal theoretical structure the cladding of the fiber is composed of seven rings of holes in a glass, ordered in a hexagonal lattice with the lattice constant $\Lambda = 1.8$ μm and the relative air-hole size $d/\Lambda = 0.91$, where d is the diameter of the holes. The real fiber was developed using the stack-and-draw technique. The final fiber has the core whose diameter equals 1.90 ± 0.08 μm. Photonic lattice of the cladding consists of 7 rings of air-holes, with the lattice constant 1.71 and the relative air-hole size equal to 0.9. According to the SEM image shown in Fig. 20, the total diameter of the inclusion was equal approximately 490 nm (a diameter at full-width half maximum FWHM of approx. 400 nm). We verified the uniformity of the drawn fiber over a distance of 20 m. In particular, the inclusion keeps the total diameter of 490 nm with an accuracy of approximately ± 10 nm.

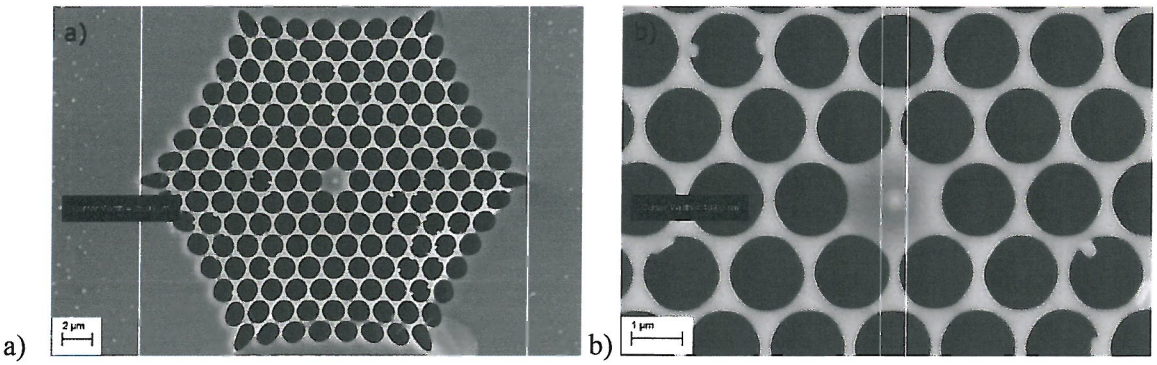

Fig. 20. SEM images of the final fiber with the inclusion diameter of approximately 490 nm.

The dispersion characteristics for the fundamental mode and for the second guided mode of the fiber with a 490 nm inclusion in the core was measured with white light interferometric method using unbalanced Mach-Zehnder interferometer. The ZDW of the fundamental mode (FM) was located at about 817 nm, while for the second order mode the ZDW equalled 606 nm. Unexpectedly, these values were very close to those obtained numerically for an ideal structure designed without any inclusion (see Fig. 21). The ZDW of the fundamental mode in this case was equal to 790 nm. It means that we observe only a 30 nm red-shift of the ZDW due to the presence of an inclusion, instead of a 650 nm red-shift.

Although these results showed that the developed structure of the photonic cladding is very similar to the ideal one, since both dispersion lines almost overlap in the whole considered wavelength range, it does not explain the huge discrepancy between the measured characteristics of the fiber and the modelled one with a 400 nm step-index inclusion in the core, determined on the basis of the SEM image.

We also considered a Gaussian profile of the inclusion instead of a step index one. In this approach, the refractive index varied from the value for the pure SF6 glass in the center, towards the value for NC21 glass at the edge of the inclusion. FWHM of this inclusion was equal to 400 nm. Although this model should incorporate the effect of the uniform diffusion of atoms and molecules from the area of the inclusion to the NC21 core of the fiber, we found that the dispersion characteristics are still far from the measured results.

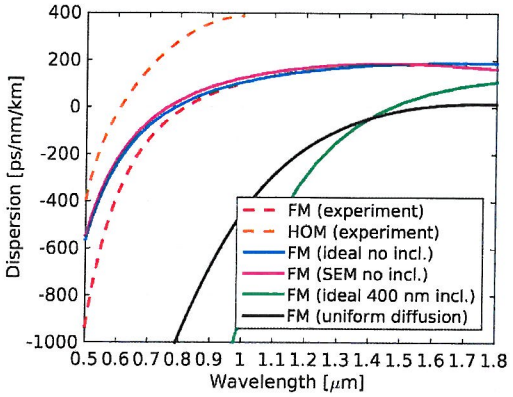

Fig. 21. Dispersion characteristics for the experimentally measured modes (dotted lines) and for the modelled fundamental modes for PCFs without an inclusion (ideal or based on SEM image), with a step-index inclusion of diameter equal to 400 nm and for the uniform model of diffusion. FM – fundamental mode, HOM – high order mode.

Both glasses used in this work, that is SF6 and NC21, have different concentrations of chemical elements O, Si and Pb. **The concentrations were measured using energy dispersive X-ray spectroscopy (EDS) implemented in Zeiss Sigma SEM.** Figures 22(a) and 22(b) present the profiles of the concentration of chemical elements expressed in weight percentage, determined along the diameter of the core of the subpreform and the final fiber, respectively. **We observed that the concentration of lead (Pb) in the area of the inclusion in the fiber drops from approx. 60% to less than 8% with respect to the central part of the subpreform core. Moreover, the inclusion was highly diffused.** Its profile is not step-index, as is the case of the subpreform, but it is close to a Gaussian profile. The ratio between the inclusion and the core diameter grows from approximately 0.14 to 0.37, which indicates the spreading of Pb atoms. This behaviour can be explained in terms of different melting point temperatures of both glasses. Because the viscosity of SF6 glass is lower than that of NC21 glass at the drawing temperature, the inclusion made of SF6 glass is softer than the core made of NC21 glass. As a consequence, SF6 glass more easily penetrates its surroundings. The EDS measurements also indicated that the concentration of oxygen (O_2), silica (Si) and sodium (Na) in the center of the subpreform is much lower than for the final fiber. Indeed, the amount of these elements in SF6 and NC21 glasses is different. However, after the fiber drawing process, the contrast in the concentration of elements between the glasses drops and it is almost imperceptible for Si and Na.

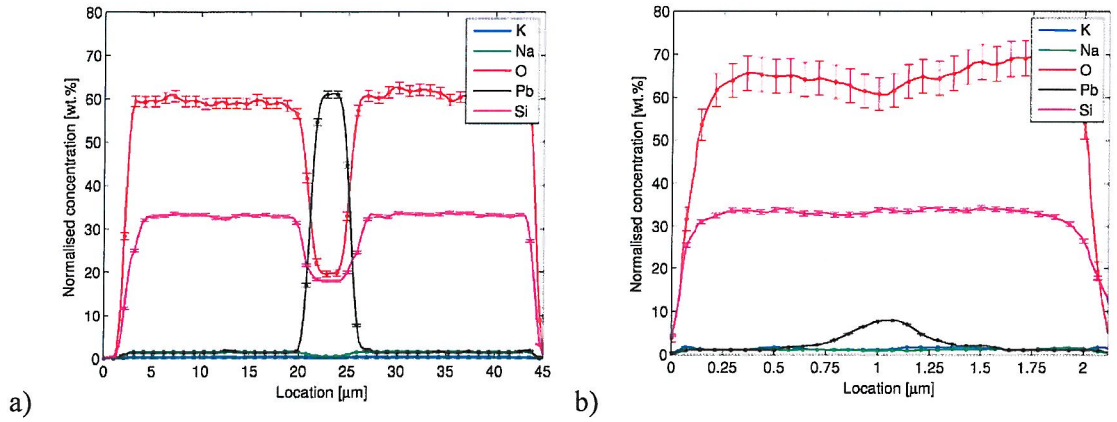

Fig. 22. The characteristics of the concentration of chemical elements along the core diameter of a) the subpreform and b) the final developed PCF.

The observations we made demonstrated a strong diffusion process in the nanoscale. They also revealed that apart from a uniform diffusion process of all components, we might also expect a non-uniform, nonselective diffusion of individual chemical ingredients in the sub-micron scale features of the fiber structure. Thus, in order to estimate the refractive index distribution in the core and the influence of uniform and non-uniform diffusion processes on the optical behaviour of the fiber, we implemented a numerical retrieval method. We assumed that the refractive index characteristic changes along the diameter of the core according to the real lead concentration, and its value changes from a hypothetical glass in the center of the inclusion to NC21 at its edge. Then, the material dispersion of this postulated glass was calculated by an optimization procedure in which the numerically calculated dispersion was compared with the measured dispersion of the fundamental mode of the PCF. In Fig. 23 the dispersion of the refractive index is plotted for SF6, NC21 glasses and also for the postulated inclusion glass.

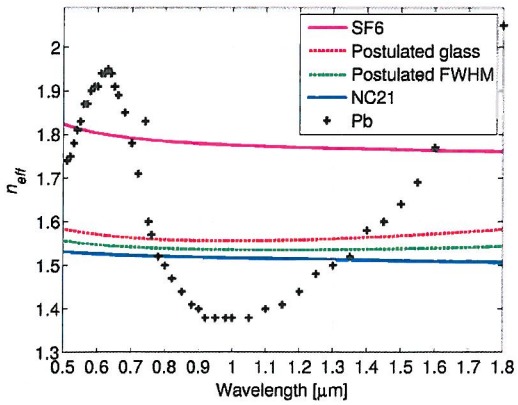

Fig. 23. Refractive index of glasses: SF6, NC21, the postulated glass, and of pure lead.

Finally, in Fig. 24 we compared the experimentally measured dispersion characteristics with the ones obtained numerically for the structure containing the postulated glass in the inclusion. Although the optimization procedure was performed only for the fundamental mode, we observe a very good agreement between numerical calculations and experimental data for the higher order mode. **This result proved the correctness of our model and confirms the fact that both the material dispersion and the refractive index of the nanoscale elements might be different than that for bulk materials.**

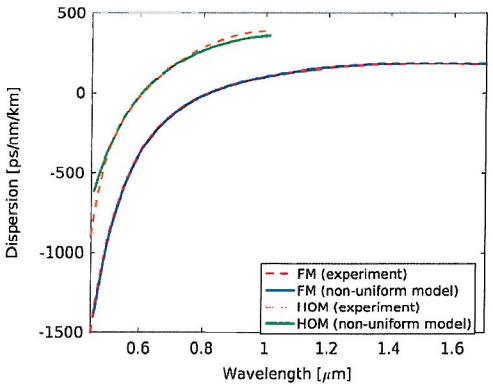

Fig. 24. Dispersion as a function of wavelength for two measured modes (dotted lines) and for modelled modes on the basis of the postulated glass.

In conclusion, we reported on the limits related to the development of fibers with a subwavelength inclusion in the core. We numerically confirmed that the PCF structure exhibits a high sensitivity of dispersion characteristics to parameters of the inclusion in the core and enables to engineer the ZDW location in a broad range, while maintaining small fundamental mode area. The experimental results showed that the profile of the inclusion in the subpreform is not maintained after the final drawing. We observed a high migration of chemical molecules in the nanoscale elements during the fiber fabrication process. **Our final note was that the diffusion and evaporation of chemical molecules for a given pair of glasses can be minimized by the optimization of technological parameters of the stack-and-draw method.** These parameters would include the lowering of the processing temperature at all stages and the increase of the fiber drawing rate. An alternative approach would be the reduction of the number of drawing stages by optimizing the stacking stage. In addition, another set of thermally matched glasses can be used. In this case, a high-index glass with a higher viscosity in the drawing temperature should be used for the inclusion, and the glass with the lower viscosity as the background glass.

The paper **[JP-6]** was selected by Optical Society of America as a Highlighted Article from OSA Journals in September 2015. It was underlined that "*in this work, the high index inclusion not only permits a tailoring of the fiber's dispersion but also a direct route to study the diffusion of the inclusion's glass components during fabrication. As such, the work sheds light – forgive the pun – on both the role of structure and materials on the performance of these interesting fibers.*"

In the subsequent paper **[JP-7]** a numerical study of the dispersion characteristic modification of nonlinear photonic crystal fibers infiltrated with liquids was presented. Prior to publishing of our paper several earlier works discussed the possibility of using liquids in PCFs. It was clear that it is usually difficult to modulate optical properties of a PCF to make it a tunable optical device. The possibility of infiltrating PCFs with liquids gives an additional degree of freedom during the design that was shown by [Ebnali-Heidari, 2012]. Particularly, the dispersion properties of the fibers can be tuned by selective hole filling [Maji, 2014]. For some liquids, e.g., liquid crystals, control of their refractive index by means of temperature in a broadband range is possible, which allows for further modification of the guiding properties of the fibers on the fly [Rasmussen, 2006]. Liquids have a relatively high nonlinear refractive index in comparison to solids, which makes it easier to observe nonlinear phenomena, such as optical solitons. For example, the nonlinear refractive index of the nitrobenzene equals 3.2×10^{-18} m^2/W at 1032 nm, while in case of the fused silica it is equal to 2.74×10^{-20} m^2/W at 1053 nm [Kedenburg, 2014]. One of the most important nonlinear phenomena is supercontinuum generation (SG). There have been several

reports on SG in liquids or in liquid-infiltrated PCFs, e.g. [Vieweg, 2010]. There was also a certain demand for optofluidic devices working in the mid-IR. Particularly, identification of biochemicals and tracing of toxic molecules are commonly conducted in this range of wavelengths [Barth, 2007]. Moreover, the invention of new light sources, such as quantum cavity lasers [Pierściński, 2015], stimulates the development of new types of PCFs working in the mid-IR.

Before our paper other publications on dispersion engineering focused mostly on fused silica PCFs. **We proposed a PCF based on soft glass PBG-08, infiltrated with different liquids. The novel feature of our work was the possibility of engineering the dispersion of a real fiber made of soft glasses through infiltration with organic liquids, when the attenuation of real liquids is taken into account.** The glass transmits light in the visible–mid-IR range of 0.4–5 μm and has a higher refractive index than fused silica, which gives higher contrast between the PCF and the liquids. The fiber was designed and then developed in the stack-and-draw process. The schematic of the fiber, and SEM image of the developed fiber is shown in Fig. 25. The PCF was made of PBG-08 glass that has a high refractive index, a high nonlinear refractive index, and good rheological properties that allow for thermal processing of the glass without crystallization. It is a lead-bismuth-galate glass.

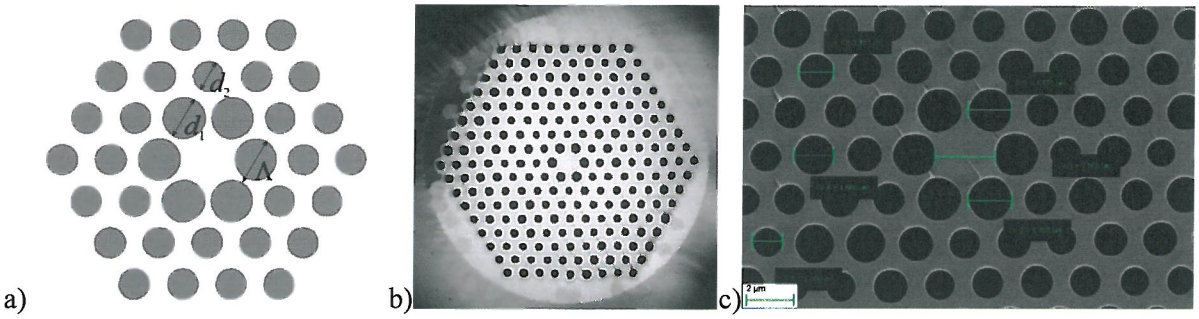

Fig. 25. a) Schematic of the developed PCF. The first three rows of holes are shown. The diameters of the holes are denoted as d_1 for the first row and as d_2 for the outer rows; Λ is the lattice constant. The linear filling factor is calculated as the ratio d/Λ. b) SEM image of the developed sub-preform. (c) SEM image of the final fiber.

It is worth noting that there were and still are certain limitations in the numerical modeling of PCFs infiltrated with liquids, due to the fact that the properties of the liquids, especially the real and imaginary parts of the refractive index, are available only for a limited wavelength range, mainly in the visible range. On the other hand, absorption losses in a broad range, including near- and mid-infrared, are important when soft glasses are used. Thus, the prediction of guiding properties in the mid-IR is difficult.

The developed fiber was investigated numerically, based on SEM images with the assumption that the air–holes are filled with a number of different liquids. For reference, the fiber with air holes only was also analysed. The list of liquids is shown in Table 2. In Fig. 26 refractive indices of the liquids are plotted.

Table 2. List of liquids used in numerical simulations.

with unknown absorption losses	with known absorption losses
1. methanol	1. water
2. acetonitrile	2. heavy water
3. 1-propanol	3. ethanol
4. isobutanol	4. chloroform
5. 1-butanol	5. toluene
6. isoamyl alcohol	6. carbon tetrachloride
7. amyl alcohol	

with unknown absorption losses	with known absorption losses
8. 1,4 dioxane 9. 1,5 pentanediol 10. benzene 11. nitrobenzene	

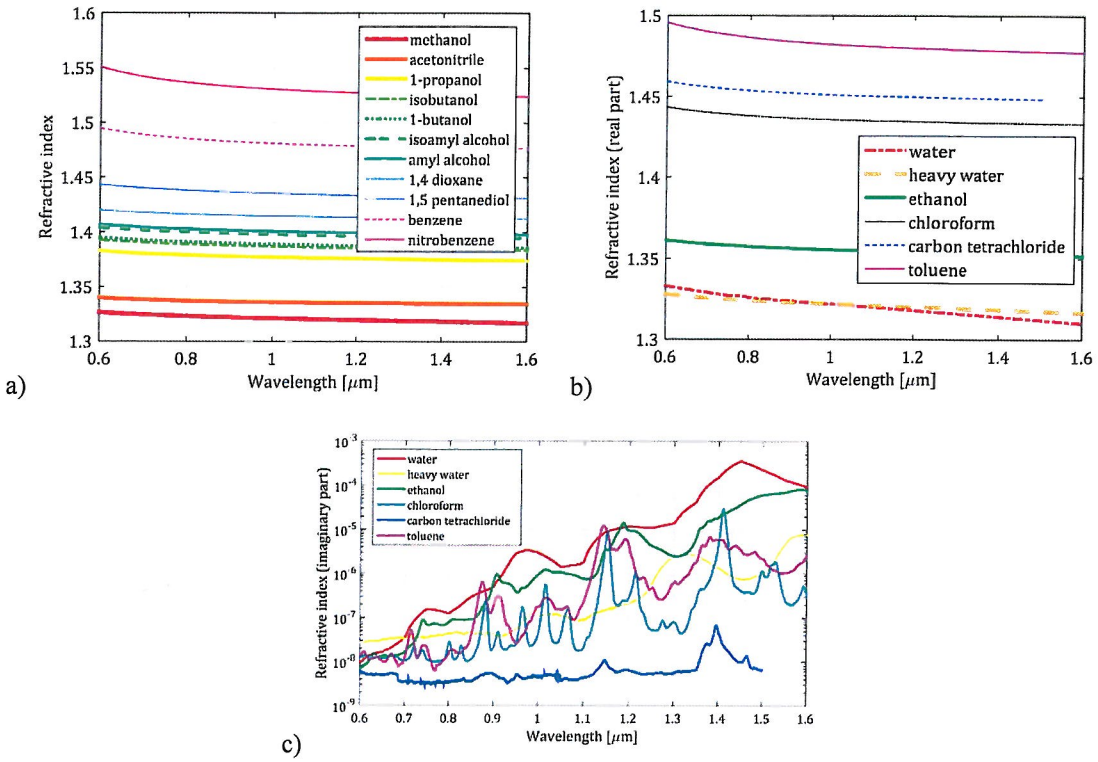

Fig. 26. a) Refractive index as a function of wavelength for liquids with unknown absorption losses. b) Real and (c) imaginary parts of the refractive index as a function of wavelength for liquids with known absorption losses.

We have calculated the dispersion as a function of the wavelength in the range of 0.6–1.6 μm, for the simulated fiber filled with the liquids having unknown losses. The characteristics are plotted in Fig. 27. The ZDW for the PCF with air–holes only is equal to 1.355 μm, and the slope of the characteristic in the vicinity of the ZDW equals approximately 2.43 ps·nm^{-2}·km^{-1}. When the holes are filled with liquids with unknown absorption losses, the ZDW is shifted toward longer wavelengths, with a decreasing slope for the dispersion characteristic. The most significant ZDW shift is observed for nitrobenzene (to 1.512 μm), while the least is observed for methanol (to 1.413 μm). In case of liquids with known losses, the presence of water shifts the ZDW up to 1.407 μm, while for toluene, the value is up to 1.484 μm. The shift allows matching the ZDW to available fiber lasers used for SG. It is well known that the most effective SG occurs when the pump wavelength is located near the ZDW on the anomalous dispersion side.

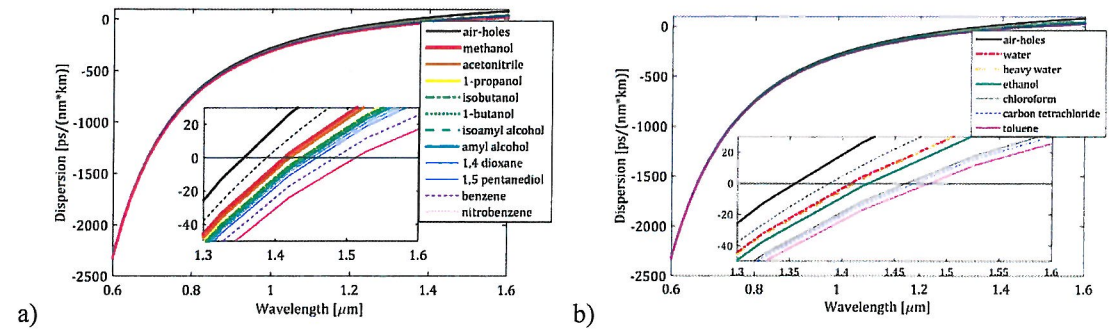

Fig. 27. Dispersion of the fiber filled with liquids, for which losses are a) unknown and b) known. In the inset, the wavelength range of 1.3–1.6 μm is enlarged. The black dash line denotes the dispersion characteristic obtained in an experiment for the fiber without liquid.

Dispersion is not the only factor that determines the effective nonlinear medium for SG. The second issue is maintaining a small mode area. Putting in the PCF a liquid with a refractive index close to that of the structure material implies spreading of the mode and thus lowering of the nonlinearity. To limit the mode area, it is beneficial to use soft glass with a high refractive index. In addition, the nonlinearity of a high index glass is much higher than that of fused silica. We calculated the mode area of the fundamental mode as a function of the wavelength in the range of 0.6–1.6 μm for the simulated fiber filled with the liquids. For the wavelength equal to 0.8 μm, the mode area was equal 3.185 μm^2 for the fiber with air holes only. When the fiber is filled with any liquid, the mode area increases. The smallest increase is observed for methanol (3.283 μm^2, that is, 3.1%), and the biggest for nitrobenzene (3.416 μm^2, that is, 7.3%). For the wavelength equal to 1.6 μm, the mode area increases from 3.558 μm^2 for air holes to 3.797 μm^2 for methanol (that is, 6.7%) and to 4.124 μm^2 for nitrobenzene (that is, 15.9%). **It is clear that the increase in the mode area is relatively small, which is beneficial for nonlinear applications.**

We calculated the attenuation of the fiber as a function of wavelength for the fiber filled with liquids with known absorption losses. The losses maintain an overall tendency to increase with increasing wavelength. The highest losses are observed for fibers infiltrated with water that is 0.013 dB/m for 0.8 μm and 37 dB/m for 1.6 μm. The lowest losses are observed for carbon tetrachloride that is 5.1×10^{-4} dB/m for 0.8 μm and 1.8×10^{-2} dB/m for 1.6 μm. **The losses at this level do not limit the SG because, when soft glasses are used, SG can be achieved in a fiber sample only a few centimeters long.**

Since the absorption losses for the liquids are much higher than for the glass, only filling the air holes in the cladding, and not the core, should be considered. In this way, the fundamental mode is not suppressed as much as the higher order modes, which is advantageous because higher order modes are usually present in small-core PCFs.

To further investigate the influence of the infiltration of the PCF on its nonlinear performance, we compared the SG performance for the fiber structures with and without liquids, using numerical simulations. The simulations were performed by GNLSE method. The simulated cases included the PCF with unfilled air holes and the PCF structure with air holes filled with toluene. The pump pulse assumed in the simulations was Gaussian-shaped and lasted 100 fs (complex amplitude), and the in-coupled energy was 0.5 nJ. As shown in Fig. 27, the difference in the ZDW location between the unaltered PCF (air holes) and the toluene-filled PCF is roughly 130 nm. Therefore, even for 100 fs pumping, which is typically dominated by self-phase modulation, the difference in supercontinuum generation performance should be noticeable. Some results of the numerical simulations for the two considered structures are shown in Fig. 28.

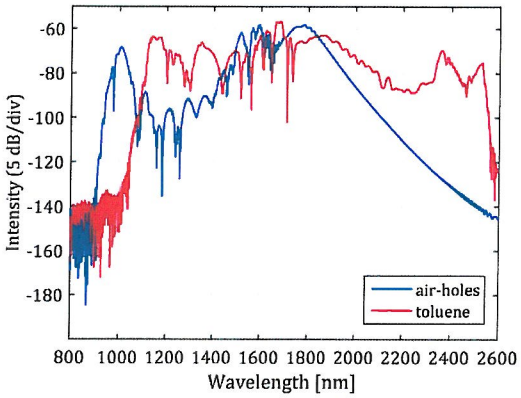

Fig. 28. Numerical simulations of the supercontinuum spectra in the PCF with air holes and toluene filled.

As an additional feature, we found that it is possible to control the ZDW and the shape of the dispersion characteristic of a liquid-filled PCF by changes in the temperature because the refractive index of the liquids change with temperature much more than those of the glasses.

Literature (excluding papers of the Applicant's cycle of research publications)

[Bartelt, 2007] H. Bartelt, J. Kirchhof, J. Kobelke, K. Schuster, A. Schwuchow, K. Mörl, U. Röpke, J. Leppert, H. Lehmann, S. Smolka, M. Barth, O. Benson, S. Taccheo, C. D'Andrea, "Preparation and application of functionalized photonic crystal fibers," Physica Status Solidi A 204(11), 3805–3821 (2007).

[Buczyński, 2011] R. Buczynski, D. Pysz, R. Stepien, A.J. Waddie, I. Kujawa, R. Kasztelanic, M. Franczyk, and M.R. Taghizadeh, "Supercontinuum generation in photonic crystal fibers with nanoporous core made of soft glass," Laser Physics Letters 8(6), 443–448 (2011).

[Feng, 2003] X. Feng, T. Monro, P. Petropoulos, V. Finazzi, and D. Hewak, "Solid microstructured optical fiber", Opt. Express 11(18), 2225–2230 (2003).

[Argyros, 2005] A. Argyros, T. Birks, S. Leon-Saval, C.M. Cordeiro, F. Luan, P. St. J. Russell, "Photonic bandgap with an index step of one percent," Optics Express 13, 309–14 (2005).

[Camerlingo, 2010] A. Camerlingo, X. Feng, F. Poletti, G. M. Ponzo, F. Parmigiani, P. Horak, M. N. Petrovich, P. Petropoulos, W. H. Loh, D. J. Richardson, "Near-zero dispersion, highly nonlinear lead-silicate W-type fiber for applications at 1.55μm," Optics Express 18(15), 15747-15756 (2010).

[Ghosh, 2010] S. Ghosh, R. K. Varshney, B. P. Pal, G. Monnom, "A Bragg-like chirped clad all-solid microstructured optical fiber with ultra-wide bandwidth for short pulse delivery and pulse reshaping," Optical and Quantum Electronics 42(1), 1–14 (2010).

[Domachuk, 2008] P. Domachuk, N. A.Wolchover, M. Cronin-Golomb, A. Wang, A. K. George, C.M.B. Cordeiro, J.C. Knight, F. G. Omenetto, "Over 4000 nm Bandwidth of Mid-IR Supercontinuum Generation in Sub-Centimeter Segments of Highly Nonlinear Tellurite PCFs," Optics Express 16(10), 7161–7168 (2008).

[Cohen, 1985] L. G. Cohen, "Comparison of single-mode fiber dispersion measurement techniques," Journal of Lightwave Technology 3(5), 958–966 (1985).

[Didams, 1996] S. Diddams, J.-C. Diels, "Dispersion measurements with white-light interferometry," Journal of the Optical Society of America B 13(6), 1120–1129 (1996).

[Hlubina, 2007] P. Hlubina, M. Szpulak, D.Ciprian, T. Martynkien, W. Urbanczyk, "Measurement of the group dispersion of the fundamental mode of holey fiber by white-light spectral interferometry," Optics Express 15(18), 11073–11081 (2007).

[Koshiba, 2003] M. Koshiba, K. Saitoh, "Finite-element analysis of birefringence and dispersion properties in actual and idealized holey-fiber structures," Applied Optics 42(31), 6267–6275 (2003).

[Ebnali-Heidari, 2012] M. Ebnali-Heidari, F. Dehghan, H. Saghaei, F. Koohi-Kamali, and M. K. Moravvej-Farshi, "Dispersion engineering of photonic crystal fibers by means of fluidic infiltration," Journal of Modern Optics 59(16), 1384–1390 (2012).

[Maji, 2014] P. S. Maji and P. R. Chaudhuri, "Design of ultra large negative dispersion PCF with selectively tunable liquid infiltration for dispersion compensation," Optics Communications 325, 134–143 (2014).

[Rasmussen, 2006] P. D. Rasmussen, J. Lægsgaard, and O. Bang, "Chromatic dispersion of liquid-crystal infiltrated capillary tubes and photonic crystal fibers," Journal of Optical Society of America B 23(10), 2241–2248 (2006).

[Kedenburg, 2014] S. Kedenburg, A. Steinmann, R. Hegenbarth, T. Steinle, and H. Giessen, "Nonlinear refractive indices of nonlinear liquids: wavelength dependence and influence of retarded response," Applied Physics B 117(3), 803–816 (2014).

[Vieweg, 2010] M. Vieweg, T. Gissibl, S. Pricking, B. T. Kuhlmey, D. C. Wu, B. J. Eggleton, H. Giessen, "Ultrafast nonlinear optofluidics in selectively liquid-filled photonic crystal fibers," Opt. Express 18(24), 25232–25240 (2010).

[Barth, 2007] A. Barth, "Infrared spectroscopy of proteins," Biochimica et Biophysica Acta (BBA) - Bioenergetics 1767(9), 1073–1101 (2007).

[Pierściński, 2015] K. Pierściński, D. Pierścińska, M. Pluska, P. Gutowski, I. Sankowska, P. Karbownik, A. Czerwiński, M. Bugajski, "Room temperature, single mode emission from two-section coupled cavity InGaAs/AlGaAs/GaAs quantum cascade laser," Journal of Applied Physics 118(13), 113103 (2015).

[Biancalana, 2010] F. Biancalana, T. X. Tran, S. Stark, M. A. Schmidt, and P. St. J. Russell, "Emergence of Geometrical Optical Nonlinearities in Photonic Crystal Fiber Nanowires," Phys. Rev. Lett. 105(9), 093904 (2010).

[Kibler, 2007] B. Kibler, P.-A. Lacourt, F. Courvoisier, and J. M. Dudley, "Soliton spectral tunnelling in photonic crystal fiber with sub-wavelength core defect," Electron. Lett. 43(18), 967–968 (2007).

[Euser, 2011] T. G. Euser, M. A. Schmidt, N. Y. Joly, C. Gabriel, C. Marquardt, L. Y. Zang, M. Förtsch, P. Banzer, A. Brenn, D. Elser, M. Scharrer, G. Leuchs, and P. St. J. Russell, "Birefringence and dispersion of cylindrically polarized modes in nanobore photonic crystal fiber," J. Opt. Soc. Am. B 28(1), 193–198 (2011).

[Ung, 2010] B. Ung and M. Skorobogatiy, "Chalcogenide microporous fibers for linear and nonlinear applications in the mid-infrared," Opt. Express 18(8), 8647–8659 (2010).

[Buczyński, 2011] R. Buczynski, D. Pysz, R. Stepien, A. J. Waddie, I. Kujawa, R. Kasztelanic, M. Franczyk, and M. R. Taghizadeh, "Supercontinuum generation in photonic crystal fibers with nanoporous core made of soft glass," Laser Phys. Lett. 8(6), 443–448 (2011).

6. Optical devices based on photonic crystal fibers

The papers **[JP-8]** and **[JP-9]** focus on applications that are optical devices based on PCFs or developed in the stack-and-draw technological process.

In the paper [JP-8] we presented a novel method for the development of diffractive optical elements (DOEs). Unlike standard surface relief DOEs, the phase shift is introduced through a refractive index variation achieved by using different types of glass.

Diffractive optics has quite a long history and offer substantial advantages over conventional refractive optics thanks to their flexibility, light weight, and planar geometries [Kress, 2000]. They found applications in optical communications, imaging and lithography, biomedical devices and optical sensors.

Prior to our publication most of the standard diffractive optical elements (DOEs) were fabricated using microlithographic techniques [Sinzinger, 1999] to create a surface relief phase profile that diffracts the incident light. This technology was well established, commercially available, and allowed for the fabrication of DOEs in a wide range of optical materials, such as glasses and polymers. Such DOEs work effectively for monochromatic illumination. This method is low cost when mass production is considered, although a single expensive mask is required. Direct laser writing techniques [Ihlemann, 2002], where a femtosecond laser is used to shape the surface of the optical material became more popular. This technique does not require a photolithographic mask but is time consuming, as the DOE is written sequentially step by step. Another group of techniques used in the fabrication of DOEs were

those based on the modification of the refractive index while preserving the flat surface of the optical materials, e.g. ion exchange method [Salmio, 1997], ion implantation [Vasquez, 2016] or glass thermal poling [Rusan, 2010], but the gradient (phase contrast) and/or depth obtained was low ($\Delta n \sim 0.01$ for soda lime glass) and the choice of materials was limited since ion exchange works efficiently for Na+ and Ag+ ions only. Another drawback of the mentioned methods was the relatively high price.

In the paper [JP-8] we proposed a new method of DOE development in which the diffraction structure is composed of "pixels" made of different types of glass, and the phase shift results from different refractive indices between pixels. Our method utilizes the low-cost modified stack-and-draw technique. In this technique, glass rods are stacked together to make a pre-form that is subsequently drawn in a furnace [Martynkien, 2014]. Each rod constitutes a single pixel and the whole structure forms a diffraction pattern when illuminated. In earlier papers published by our group the possibility of using the stack-and-draw technique for the fabrication of nanostructured gradient index microlenses [Hudelist, 2009] and nanostructured birefringent elements [Waddie, 2011] was demonstrated.

In the proof-of-concept demonstration, two types of glass were used, although it is possible to use a virtually unlimited number of glasses if they are thermally matched and can be jointly processed. **The presented method allows for the creation of arbitrary patterns with a smallest feature size of tens of nanometers—the lower limit of the feature size is set by the diffusion of molecules during the drawing of fibers [JP-6].** Moreover, our DOEs have completely flat surfaces, can be cut and polished to the desired phase contrast, are robust, and are easy to integrate with other optical components, e.g., fibers. **The cost of our method is comparable with the cost of the ion-exchange method and can be even lower when a large quantity of DOEs is required.**

The proof-of-concept demonstration consisted of design, numerical modelling, development, and experimental verification. A two dimensional binary optical phase grating in the form of a chessboard with a square lattice had been proposed (see Fig. 29). The structure might be used as a beam splitter in optical fiber systems, for example, for the addressing an array of cores in a multicore fiber.

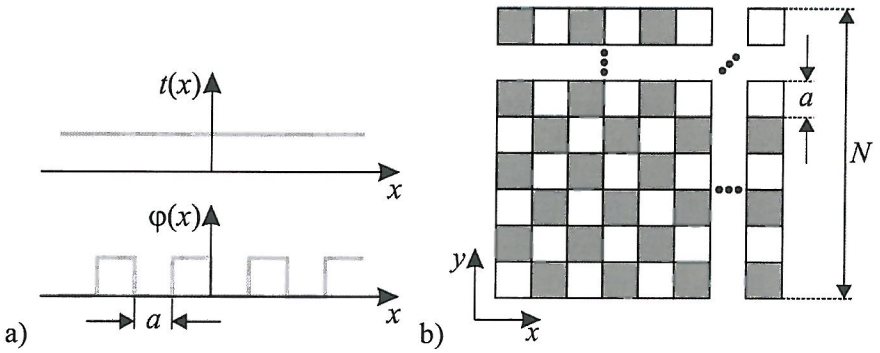

Fig. 29. The phase transmittance of (a) a one-dimensional and (b) two-dimensional quasi-infinite binary optical phase grating.

The optical transmittance of this chessboard is given by the equation

$$g(x,y) = P\left\{\left[\mathrm{comb}\left(\frac{x}{a},\frac{y}{a}\right)\exp[i\varphi(x,y)]\right]\right\} \otimes \left[\mathrm{rect}\left(\frac{x}{a},\frac{y}{a}\right)\right],$$

where the amplitude transmittance $t(x,y)$ is set to 1, a is the lattice constant and at the same time the size of a single square, and $\otimes$ denotes the convolution operator. Making use of the convolution theorem and assuming that there are N squares in each direction in the aperture, the distribution of light intensity for

the illumination with a plane wave in one direction ($y = 0$) takes the form below, and is shown in Fig. 30,

$$I(x') = \frac{1}{N^2}\left|\frac{\sin(N\Delta\varphi ax')}{\sin(\Delta\varphi ax')}\right|^2 \operatorname{sinc}^2(\Delta\varphi ax').$$

In our case of a binary phase grating in the form of a square chessboard all even diffraction orders ($m = \pm 2, \pm 4, \ldots$) are equal to zero, while the intensity of odd diffraction orders ($m = 0, \pm 1, \pm 3, \ldots$) depends on the phase difference $\Delta\varphi$. The equations for calculation of a few first diffraction orders for 2D chessboard with an arbitrary phase shift $\Delta\varphi$ are presented in Table 3. When the phase shift equals π, the total energy directed into four peaks located at in $\bar{1}0,0\bar{1},10,01$ diffraction orders equals 81% of the input energy.

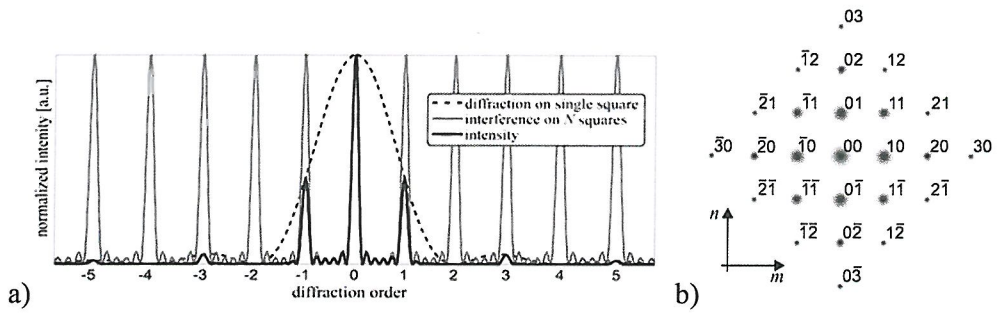

Fig. 30. Schematics of the interference pattern on (a) a one-dimensional square chessboard, and (b) two-dimensional square chessboard, with $N = 6$. The overlines represent negative orders.

Table 3. Intensity of the diffraction orders (m,n) of a binary phase 2D grating with the phase shift $\Delta\varphi$.

Diffraction order	**arbitrary $\Delta\varphi$**	**$\Delta\varphi = \pi$**
I_{00}	$\cos^4\left(\frac{\Delta\varphi}{2}\right)$	0
$I_{\pm m,0}$, $I_{0,\pm n}$ (odd m,n)	$\frac{4}{\pi^2 m^2}\sin^2\left(\frac{m\Delta\varphi}{2}\right)$	$\frac{4}{\pi^2 m^2}$
$I_{\pm m,0}$, $I_{0,\pm n}$ (even m,n)	0	0
$I_{\pm m,\pm n}$ (odd m,n)	$\frac{16}{\pi^4 m^2 n^2}\sin^2\left(\frac{m\Delta\varphi}{2}\right)\sin^2\left(\frac{n\Delta\varphi}{2}\right)$	$\frac{16}{\pi^4 m^2 n^2}$
$I_{\pm m,\pm n}$ (even m,n)	0	0

The theoretical analysis presented above can be extended with the numerical modelling of a more realistic setup, where the illuminating wave is Gaussian, and not plane. The analysed DOE is located in the setup shown in Fig. 31, with a thickness of 100 μm, composed of two materials of different refractive index that is 1.5 and 1.51. The size of a single square (pixel) is equal to 5 μm. A Gaussian source is used with the beam waist diameter equal to 10 μm and the wavelength equal to 1550 nm. The waist is located 10 mm in front of the lens L (focal length = 25 mm). The observation screen S is 25 mm away from the lens.

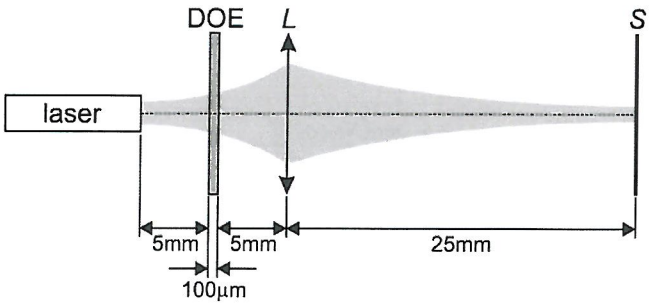

Fig. 31. The schematic of the numerical simulation setup.

Figure 32 shows the intensity distributions calculated for the plane of the screen. It is clear that the even diffraction orders are not equal to zero, because DOE is illuminated by a divergent wave. This affects the optical path difference within each pixel of the DOE, and effectively makes the refractive index change not sharply binary but fuzzy at the borders between neighboring pixels. In the simulation the total light intensity observed in four diffraction orders represents 35% of the total light intensity in the diffraction plane.

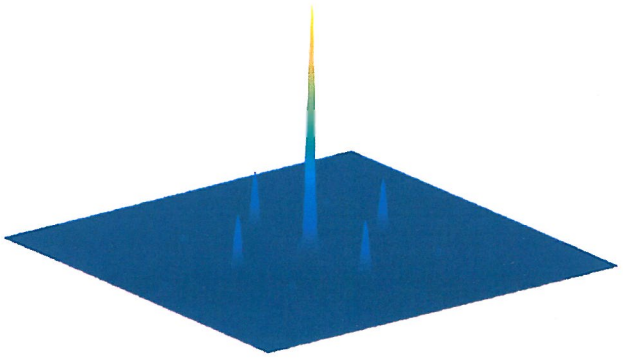

Fig. 32. The intensity distribution in the screen plane.

Based on numerical simulations, the DOE was developed in the modified stack-and-draw process that consisted of several steps as shown in Fig. 33. First, rectangular or round rods, made of different glasses and of diameter equal to approximately 1–2 mm, are stacked one-by-one according to the desired pattern and establish the initial pre-form. Each rod may correspond to a single pixel of a DOE. All rods have the identical size, therefore they can be assembled together without deformations. The number of different types of glass matches the number of phase steps in the final DOE. The next step is drawing the pre-form, which scales it down approximately 10–30 times. The obtained fiber with structures is cut into slices, grounded and polished to the required thickness which is typically tens or hundreds of microns. In this one–step process we can fabricate DOEs with the pixel size of 20–100 μm. For periodic structures, like chessboards, the obtained structured rods can be stacked again as an intermediate sub-pre-form and drawn again. As a result, DOEs with pixel sizes equal to single microns can be achieved. The size limiting factor is the diffusion process between glasses **[JP-6]**, however, to some extent this can be taken into account during the design of a DOE. **With the proposed method we can develop arbitrary structures with a large refractive index difference.**

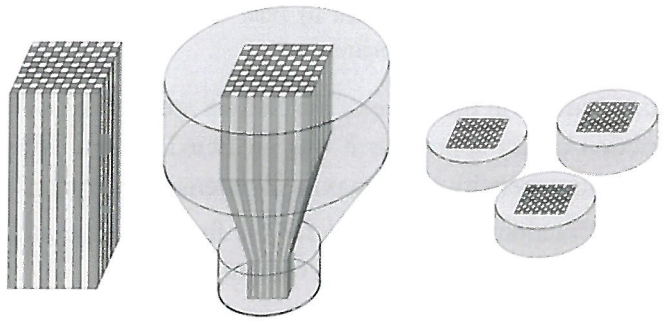

a) b) c)

Fig. 33. Schematic of the modified stack-and-draw technique. (a) a pre-form, (b) scaling down in the fiber drawing tower, (c) cut and polished DOEs.

In our real example an in-house synthesized low-index silicate glass NC21 and a commercially available high-index lead-silicate glass F2 were used. The obtained final fibers were cut and polished to achieve 100 μm-thick samples on a glass plate. We used only manual cutting and polishing tools, therefore, the accuracy of the cutting is limited. We estimated the accuracy of thickness to ±10 μm. Figure 34 presents the images of the DOE, made using a scanning electron microscope (SEM). The pixel size, that is the unit square of the chessboard, is equal to approximately 5 microns.

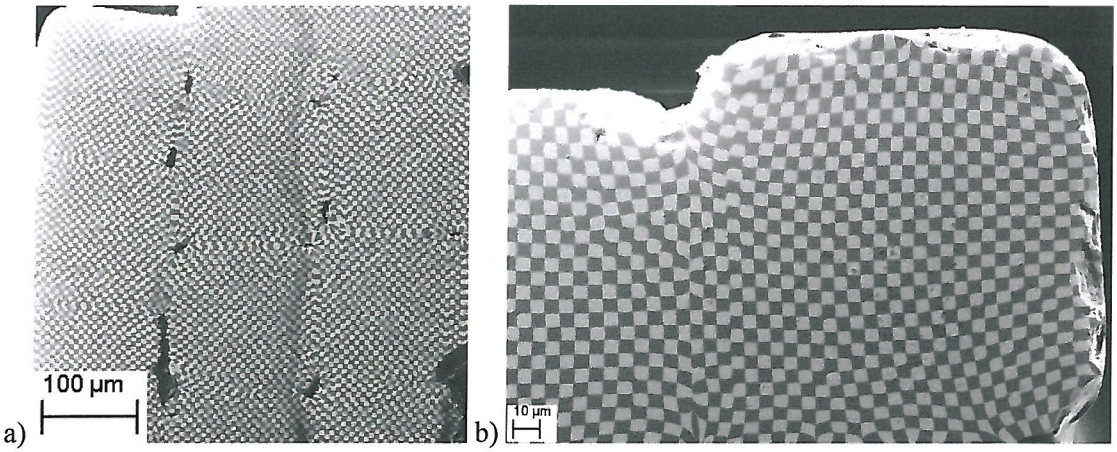

Fig. 34. SEM images of the chessboard DOE with a pixel size of 5 μm. a) chessboards combined into a single structure b) close-up of a single chessboard.

The performance of the fabricated DOE was verified by constructing two proof-of-concept demonstrations in two experimental setups shown in Fig. 35. First was a fan out setup, the second fiber multi-core interconnector setup. The details of the setups are discussed in the paper in detail.

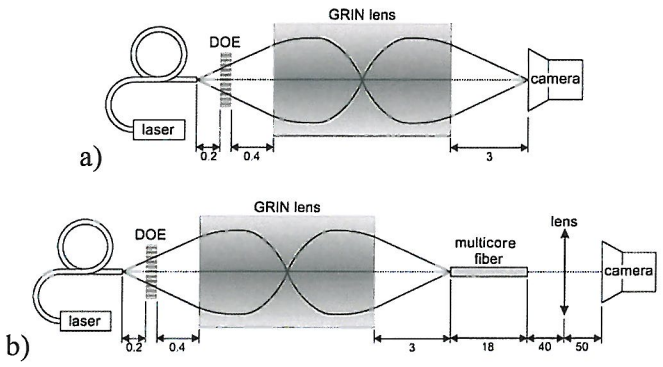

Fig. 35. Schematic of the experimental a) fan-out and b) fiber multi-core interconnector setup for the DOE characterization. B) All distances are given in millimetres.

The resulting intensity distributions in the plane of the camera are shown in Fig. 36. We observed that both even and odd diffraction orders appear, as it was predicted in simulations. We obtained regular diffraction patterns and high homogeneity of the maximum intensity in $\bar{1}0,0\bar{1},10,01$ diffraction orders. The light intensity in this four diffraction orders is 15% for the fan–out setup and 17% for the multi-core interconnector setup, of the total light intensity in the camera plane.

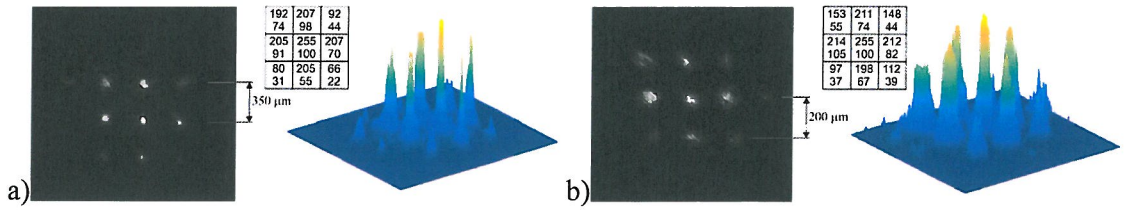

Fig. 36. Normalized intensity distribution in the plane of the camera for a) the fan-out setup and b) the multi-core fiber interconnector setup. The tables present the maximal intensity (upper numbers in the cells) and the total light intensity (lower numbers in the cells) within a 50 µm–diameter circular area surrounding each maximum, normalized to 100 for the central diffraction maximum.

As a result we demonstrated that it is possible to develop flat, easy to integrate and robust diffractive optical elements using the modified stack-and-draw technique. We have verified that the fabricated chessboards generate regular diffraction patterns and can be used as multi-core fiber interconnectors for coupling light from a small core fiber into the several cores of a multi-core fiber.

The analysis, simulation and the experiment were conducted for monochromatic and spatially coherent illumination. However, some applications may require that the DOE is illuminated using a broadband light source. The design of a DOE operating in such a manner is usually much more complicated because of chromatic aberrations and material dispersion that needs to be compensated numerically. **Since in our case the refractive index difference between the two glasses, shown in Fig. 37, is quasi-constant over the analysed range of wavelengths, this chromatic aberration is effectively decreased. Additionally, our method offers sufficient design flexibility that almost any distribution of refractive index across the DOE can be fabricated which makes it possible to use advanced optimisation methods to further reduce these chromatic aberrations.**

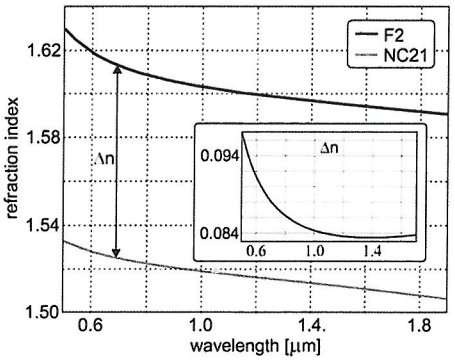

Fig. 37. The refractive index and the refractive index difference Δn as a function of the wavelength for the NC21 and F2 glasses.

In the paper [JP-9] we presented a large mode area photonic crystal fiber (LMA PCF) made of the heavy oxide glass CS-740, dedicated for a broadband light guidance in the visible, near- and mid-infrared regions of wavelengths from 0.4 to 4.7 μm. The fiber is effectively multi-mode in the considered wavelength range. It is composed of a ring of air-holes surrounding the core, with a high linear filling factor of 0.97. **We presented a proof-of-concept demonstration that our large core PCF is able to efficiently collect light directly from a mid-IR quantum cascade laser without use of additional optics and can be used for pigtailing mid-IR sources and detectors.**

Prior to the publication of our paper LMA PCFS were investigated by several authors due to their exceptional guiding properties, especially single-mode guidance in extremely large structures, low nonlinearity, strong birefringence and dispersion management ability [Knight, 1998]. These unique properties result from microstructured cladding and proper choice of glass material. High power delivery combined with possibility to collect light over large areas offered by LMA PCFs are desirable in various applications, such as optical coherence tomography, infrared spectroscopy or airborne light detection and ranging (LIDAR). Several successful approaches for the design and fabrication of LMA PCFs were reported [Tan, 2008; Napierała, 2011]. Ultra large core PCFs were proposed, having mode area of 1454 μm^2 [Matsui, 2011].

Majority of LMA PCFs were at that time made of silica glass with an air photonic crystal cladding, which limits their applications to the visible and near-infrared parts of the light spectrum. Moreover, it is difficult to enlarge the effective mode area for broadband applications, due to the trade-off relationship between fiber cut-off wavelength and bending losses. Increasing number of mid-IR sources, including new quantum cascade lasers (QCLs) and the demands of the modern spectroscopy and sensing created a need for the development of new LMA PCFs, which are capable to transmit light also in the mid-IR region, especially at wavelengths above 2 μm, and exhibit low bending losses, with good mechanical properties and high resistance to the laser damage. Standard photonic solutions cannot be used due to limited transmittance of most materials in this range of wavelengths. There was and still is a strong demand to develop pigtailed mid-IR sources and detectors, potentially easy to handle. This task can be accomplished with LMA PCFs having a large core area and a high numerical aperture, allowing to collect light directly from the source, in the on-chip configuration.

Despite significant improvements and development of mid-IR sources, there was still a problem of delivery of light to experimental setups due to a lack of efficient fibers and coupling optics. To meet the above mentioned requirements, various soft glasses, such as chalcogenide, fluoride, tellurite or heavy metal oxide glasses, can be used as an alternative to fused silica [France, 1987; Lorenc, 2008].

In this paper we presented for the first time a LMA PCF made of a heavy oxide glass CS-740, dedicated to broadband light guidance in the near- and mid-infrared regions of the optical spectrum. The fiber was made using the stack-and-draw process. Use of a soft glass has advantages over other solutions. ZBLAN fibers may be difficult to work with and are not mechanically durable, while chalcogenide glasses are toxic and expensive. Heavy metal oxide glasses are a kind of compromise choice. They are relatively cheap to make, the processing is easy and allows hot embossing, while fibers are mechanically durable and have good transmission properties. The developed fiber was analysed numerically and characterized in the near- and mid-IR ranges. Thanks to a large core and numerical aperture it is dedicated for light delivery and collection in the broad wavelength range from 0.5 to 5 μm in pigtailed optical devices, especially in on-chip configurations.

The proposed ideal fiber has a large core surrounded by a ring of air-holes of 3.2 μm diameter, shown schematically in Fig. 38. The distance between centers of adjacent holes equals 3.33 μm, which implies a high linear filling factor of approx. 0.97. Fiber core diameter is 80 μm.

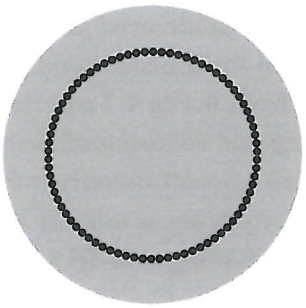

Fig. 38. Schematic of the proposed ideal LMA PCF.

To make the fiber we have used the standard stack-and-draw process. The fiber is made of in-house developed heavy oxide glass CS-740 [Stępień, 2012]. This glass offers a high transmission in the broad wavelength range of 0.5–5 μm and does not exhibit the self-darkening process, unlike common ZBLAN fibers. Fig. 39 shows the cross-section of the developed fiber, as seen by a scanning electron microscope (SEM). The holes are no longer circular but elongated in the radial direction. Diameter of the core is 72 μm, while the diameter of holes is approx. 3 μm in the radial direction and approx. 2 μm in the circumferential direction. Cladding diameter is approx. 120 μm.

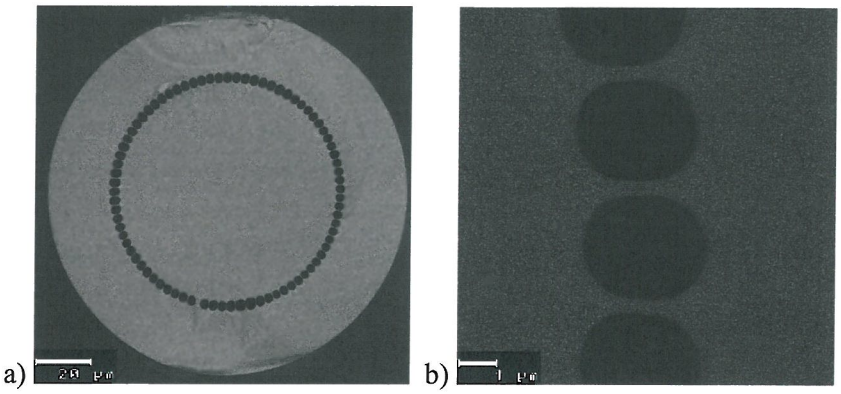

Fig. 39. SEM images of the developed fiber.

The modal and dispersion properties of this fiber were modelled numerically using the finite difference method based on the SEM image of fiber cross-section. This way, we used the real refractive index distribution of the background glass in our calculations, while including all imperfections which occurred during fiber manufacturing. Fig. 40a depicts the effective refractive index of the fundamental mode, and Fig. 40b presents the chromatic dispersion of the fundamental mode in the wavelength range of 0.5–5 μm. The fundamental mode area of the PCF is 2407 μm^2 at the 0.8 μm wavelength and 2422 μm^2 at 1.5 μm. The dispersion of the fundamental mode is close to zero across a broad spectral range.

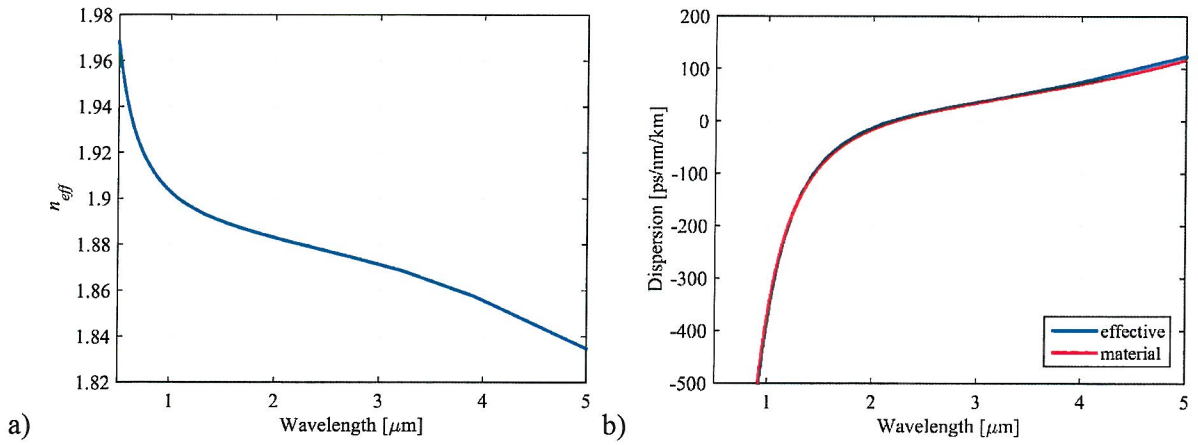

Fig. 40. The characteristics of the fiber modelled numerically on the basis of SEM images: a) effective refractive index; b) effective chromatic dispersion of the fundamental mode and material dispersion of the glass. ZDW of the effective dispersion is 2.223 μm, while of the material dispersion is 2.175 μm.

The attenuation of the modes and the effective mode area for certain modes, at wavelengths 0.8 and 4.7 μm are shown in Table 4.

Several experimental setups were used to characterise our LMA PCF. We have measured the attenuation at wavelengths in the range of 0.730–1.7 μm as well as bending losses and numerical aperture (NA) at 1.550 μm. Details of experimental setups are discussed in the paper.

PCF attenuation was measured using the cut-back technique. The beam was collimated by objectives and coupled from an SMF fiber into the fiber under test. The power coupling efficiency between SMF and the PCF tested was 68.75%. The output beam was measured with an optical spectrum analyser (OSA). Spectral characteristic of fiber attenuation is shown in Fig. 41. For the wavelength range of 1–1.4 μm, the attenuation was below 2 dB/m. At longer wavelengths it increases to approx. 2.5 dB/m, and at shorter wavelengths rises to approx. 8 dB/m at 0.73 μm.

Table 4. Attenuation and effective mode area for the guided modes at 0.8 μm and 4.7 μm. The effective mode area is estimated with uncertainty of 100 μm².

	0.8 μm		**4.7 μm**	
Mode	**Loss [dB/m]**	**A_{eff} [μm²]**	**Loss [dB/m]**	**A_{eff} [μm²]**
LP_{01}	2×10^{-11}	2400	6×10^{-8}	2400
LP_{11}	2×10^{-10}	2500	4×10^{-7}	3300
LP_{21}	2×10^{-8}	2200	2×10^{-5}	2300
LP_{02}	2×10^{-5}	1800	2×10^{-4}	1900

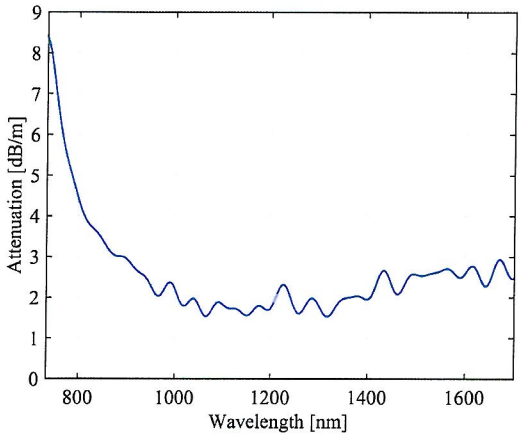

Fig. 41. Attenuation spectrum of LMA PCF measured in the 0.73–1.7 μm range.

The fiber under test was wrapped around a mandrel having a controlled radius R. Maximum bending losses in respect to straight fiber (R = ∞) reach 0.45 dB/loop for the bending radius R = 8 mm. The fiber was mechanically resistant and had low sensitivity to bending. At the wavelength 1.55 μm NA measured was approx. 0.53.

To verify the predicted numerically suitability of using our LMA PCF for pigtailing quantum cascade lasers emitting in the mid-IR range we have arranged a proof-of-concept setup, a schematic of which is shown in Fig. 42.

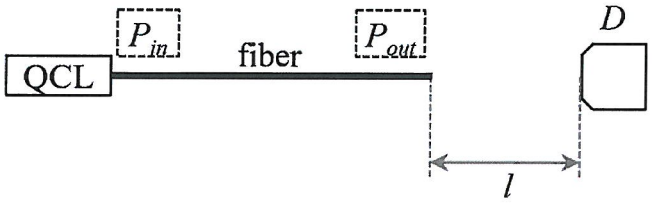

Fig. 42. Schematic of the experimental setup for the coupling efficiency measurement in mid-IR. The distance l varies in the range of 0–100 μm.

A strain-compensated quantum cascade laser (QCL), designed for emission at 4.4 μm wavelength, operating in pulsed regime was used as a source of light. The active area of the source is approx. 10×7 μm, while the NA is 0.62 in the direction of the growth of the crystal and 0.95 in the perpendicular direction. The microscopic image of those two elements of the setup and the schematic of the QCL are shown in Fig. 43. Input and output power were measured with an MCT TE cooled detector. To verify coupling efficiency we used only a short length of fiber (2 cm) to minimize influence of fiber attenuation on output power. We have measured 270 mW and 550 mW at fiber output in case of 467 mW and 933 mW total optical output of QCL. **This corresponds to coupling efficiency of approx. 58%.**

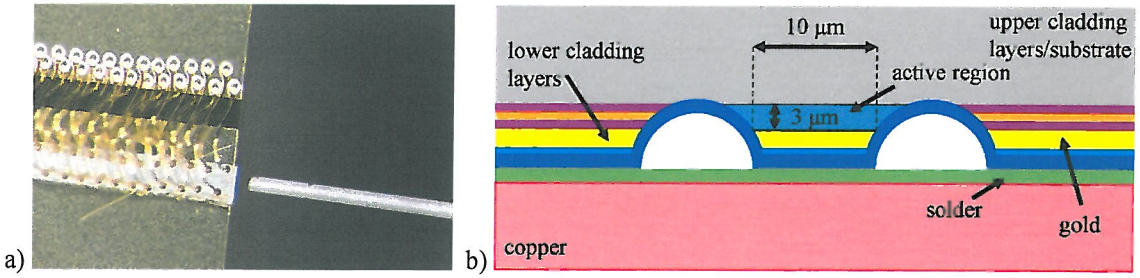

Fig. 43. a) Microscopic image of QCL and the end of fiber during movement towards the source. The outer diameter of the fiber is 120 μm. b) Structure of QCL used.

The demonstration confirmed that the newly made fiber is well suited for pigtailing of QCLs. The butt-coupling from QCL to LMA PCF is possible and effective. The CS-740 glass allows to use only few centimeters-long fibers for applications at the wavelength of 4.4 μm, since the bulk glass attenuation is approx. 5 dB/cm. This glass works best for wavelengths below approx. 2.8 μm.

Literature (excluding papers of the Applicant's cycle of research publications)

[Kress, 2000] B. Kress and P. Meyrueis, Digital Diffractive Optics: An Introduction to Planar Diffractive Optics and Related Technology (Wiley, 2000).

[Sinzinger, 1999] S. Sinzinger and J. Jahns, Microoptics (Wiley-VCH, 1999).

[Ihlemann, 2002] J. Ihlemann and D. Schafer, "Fabrication of diffractive phase elements for the UV-range by laser ablation patterning of dielectric layers," Appl. Surf. Sci. 856, 197–198 (2002).

[Salmio, 1997] R.-P. Salmio, J. Saarinen, J. Turunen, and A. Tervonen, "Gradedindex diffractive structures fabricated by thermal ion exchange," Appl. Opt. 36, 2048–2057 (1997).

[Vasquez, 2016] G. V. Vázquez, R. Valiente, S. Gómez-Salces, E. Flores-Romero, J. Rickards, and R. Trejo-Luna, "Carbon implanted waveguides in soda lime glass doped with Yb3+ and Er3+ for visible light emission," Opt. Laser Technol. 79, 132–136 (2016).

[Rusan, 2010] V. V. Rusan, D. K. Tagantsev, A. A. Lipovskii, and K. Paivasaari, "A new method for recording phase optical structures in glasses," Glass Phys. Chem. 36, 513–516 (2010).

[Martynkien, 2014] T. Martynkien, D. Pysz, R. Stępie ´ n, and R. Buczy´ nski, "All-solid microstructured fiber with flat normal chromatic dispersion," Opt. Lett. 39, 2342–2345 (2014).

[Hudelist, 2009] F. Hudelist, R. Buczynski, A. J. Waddie, and M. R. Taghizadeh, "Design and fabrication of nano-structured gradient index microlenses," Opt. Express 17, 3255–3263 (2009).

[Waddie, 2011] A. J. Waddie, R. Buczynski, F. Hudelist, J. M. Nowosielski, D. Pysz, R. Stepien, and M. R. Taghizadeh, "Form birefringence in nanostructured micro-optical devices," Opt. Mater. Express 1, 1251–1261 (2011).

[Knight, 1998] J. C. Knight, T. A. Birks, R. F. Cregan, P. St. J. Russell, and J.-P. de Sandro, "Large mode area photonic crystal fiber," Electronics Letters 34(13), 1347–1348 (1998).

[Tan, 2008] X. Tan, Y. Geng, E. Li, W. Wang, P. Wang, and J. Yao, "Characterization of bent large-mode-area photonic crystal fiber," Journal of Optics A: Pure and Applied Optics 10(8), 085303 (2008).

[Napierała, 2011]M. Napierała, T. Nasilowski, E. Bereś-Pawlik, P. Mergo, F. Berghmans, and H. Thienpont, "Large-mode area photonic crystal fiber with double lattice constant structure and low bending loss," Optics Express 19(23), 22628–22636 (2011).

[Matsui, 2011] T. Matsui, T. Sakamoto, K. Tsujikawa, S. Tomita, and M. Tsubokawa, "Single-mode photonic crystal fiber design with ultralarge effective area and low bending loss for ultrahigh speed WDM transmission," Journal of Lightwave Technology 29(4), 511–515 (2011).

[France, 1987] P. W. France, S. F. Carter, M. W. Moore, and C. R. Day, "Progress in fluoride fibers for optical communications," British Telecom Technology Journal 5(2), 28–44 (1987).

[Lorenc, 2008] D. Lorenc, I. Bugar, M. Aranyosiova, R. Buczynski, D. Pysz, D. Velic, and D. Chorvat, "Linear and nonlinear properties of multicomponent glass photonic crystal fibers," Laser Physics 18(3), 270–276 (2008).

[Stępień, 2012] R. Stepien, D. Pysz, I. Kujawa, J. Pniewski, A. J. Waddie, M. R. Taghizadeh, and R. Buczynski, "Development of large-core photonic crystal fiber for hyperspectral transmission," Proc. SPIE 8426, 842614 (2012).

7. Summary of research achievements and results obtained by the Applicant

Achievement in the field of metamaterials and plasmonic devices consists in numerical demonstration of phenomena: enhancement of a wave front incident on an interface between left– and right–handed materials, and in numerical demonstration of light focussing by a silver nanolens. The achievement encompasses results presented in the papers:

[JP-1] Demonstration for the first time that wave front of CW Gaussian beam that incidents normally on the interface between a nondispersive right–handed material (RHM) and a strongly dispersive lossy

left–handed medium (LHM) undergoes local enhancement of the power flow and shape modification of envelope of amplitudes of a group of interfering waves with different frequencies.

[JP-2] Demonstration of a phenomenon of focusing a radially polarized Laguerre-Gauss beam from the visible range by a silver film with no hole on the optical axis and double-sided concentric corrugations, based on FDTD simulations. Such a nano-lens was proposed for the first time.

Achievement in the field of photonic crystal fibers consists in proof that all–solid and liquid–filled photonic crystal fibers, made of special combination of soft glasses allow to engineer the fibers dispersion characteristics in a broad range of wavelengths due to proper design of their internal structure and choice of glasses. That allows for creation of new class of fiber–based coherent supercontinuum sources. The achievement encompasses results presented in the papers:

[JP-3] An all-solid photonic crystal fiber, made from soft glasses: SF6/LLF1, SF6/F2, or F2/NC21 was proposed, analysed numerically, and then developed in the stack-and-draw process, for the first time. The fiber parameters' control during the drawing process is much simpler than using other methods and the development of parameters similar to the designed ones is straightforward. In addition, the APCFs have unique spectral and dispersion properties that are suitable for applications in low–loss fiber lasers, nonlinear optics, birefringent fibers. The developed fiber is well optimized for supercontinuum generation in the normal dispersion regime with a source that emits at 1540 nm.

[JP-4] Demonstration of dispersion management and supercontinuum generation capabilities in high-contrast APCFs made of soft glasses (SF6/NC21) with a low index subwavelength inclusion in the core, for the first time. The inclusions make it possible to engineer the dispersion while maintaining a constant effective mode area. Demonstration of the fiber as a new efficient light source for optical coherent tomography and multiple band telecommunication applications.

[JP-5] Discussion on the reliability of dispersion measurement in APCFs, which are usually developed in short sections. Presentation of the results of the measurements of an APCF with a nanoinclusion in the core, made of SF6 and NC21 glasses, for the first time. Discussion on the differences between numerically modelled and experimentally measured dispersion characteristics of a fiber.

[JP-6] Qualitative and quantitative explanation of the discrepancy between numerically modelled dispersion characteristics and obtained experimentally, for PCFs with nanostructured cores, for the first time. The research was made on the basis of previously designed and modelled PCF with a subwavelength inclusion in the core. We showed the effect of diffusion using energy dispersive X-ray spectroscopy and proposed a model of an effective postulated glass which matches the spreading effect of molecules. We confirmed the fact that both the material dispersion and the refractive index of the nanoscale elements might be different than that for bulk materials.

[JP-7] Presentation of a numerical study of the dispersion characteristic modification of nonlinear PCFs, based on soft glass PBG-08, infiltrated with 17 different liquids. The novel feature of our work was the possibility of engineering the dispersion of a real fiber made of soft glasses through infiltration with organic liquids, when the attenuation of real liquids is taken into account. We also compared the supercontinuum generation performance for the fiber structures with and without liquids, using numerical simulations which confirmed the possibility to use this fiber with liquids to generate SC.

Achievements in the field of optical devices consists in 1) demonstration of a new method of development of diffraction optical elements, based on stack-and-draw technique, that leads to a new class of diffraction optical devices, in which arbitrary distribution of refraction index is possible; 2) demonstration of a new class of photonic crystal fibers, that can be pigtailed to modern

mid-infrared sources, such as quantum cavity lasers, and detectors. The achievement encompasses results presented in the papers:

[JP-8] Demonstration, for the first time, a new method of DOE development in which the diffraction structure is composed of "pixels" made of different types of glass, and the phase shift results from different refractive indices between pixels. The method utilizes the low-cost modified stack-and-draw technique. The proof-of-concept demonstration consisted of design, numerical modelling, development, and experimental verification. A two dimensional binary optical phase grating in the form of a chessboard with a square lattice had been proposed, modelled numerically, developed and verified in experimental setups. The structure might be used as a beam splitter in optical fiber systems, for example, for the addressing an array of cores in a multicore fiber.

[JP-9] Demonstration, for the first time, of a large mode area photonic crystal fiber (LMA PCF) made of heavy metal oxide glass CS-740 that was designed for a broadband light guidance in the near- and mid-infrared regions. Demonstration the proof-of-concept experiment that the new fiber is suitable for making pigtails to quantum cascade lasers and MCT detectors. The fiber can be used in butt-coupling configurations allowing to couple light without any optics, which is simple, inexpensive and suitable for on-chip setups. Low chromatic dispersion of the fiber allows for transmission of short pulses at infrared wavelengths for applications in dynamic chemical spectroscopy.

5. Discussion of other scientific achievements

a) achievements before obtaining the PhD degree

Before obtaining the PhD degree the Applicant scientific interest was image processing. This research was done in Department of Information Optics Department at Faculty of Physics, University of Warsaw. As a first project during the PhD studies I analysed spectral information content of satellite multispectral pictures made by the Landsat TM sensor. The main task was to classify forest areas in the north-western Poland on the basis of combined information from the multispectral Landsat image and ground truth data. The Applicant was also involved in organisation of Satellite Image Processing Laboratory in the Department.

Second project focused on mathematical morphology algorithms that implemented sub-band or pyramid decomposition of images. This algorithm was used in a lossy compression routine that was the extension of the work presented in MSc dissertation, and in a contrast deformation removal routine in grayscale images.

The third project was semi–automatic preparation that was modelling and visualisation of scalar fields on the basis of isolines. The isolines were obtained from topographical maps. This project was presented in the PhD thesis.

b) achievements after obtaining the PhD degree

After obtaining the PhD degree the Applicant was involved in several scientific projects. First projects were in the field of metamaterials and plasmonic devices in collaboration within the work group led by **prof. Tomasz Szoplik** at Faculty of Physics, Warsaw University. Next projects were carried out in the work group led by **dr hab. Ryszard Buczyński**. This work resulted in a series of publications and conference proceedings. Selected publications from Applicant's work within this two groups are the Applicant's cycle presenting the scientific achievements.

The Applicant was also deeply involved in preparation and implementation of the 3-year interdisciplinary undergraduate program *"Applications of physics in biology and medicine, course in Ophthalmic Optics and Optometry"* at Faculty of Physics. This course started in 2009. The idea and main preparation was completed by **dr hab. Marek Kowalczyk-Hernández**. In 2016 new 4-year undergraduate program *"European studies in ophthalmic optics and optometry"* was started at Faculty of Physics. Marek Kowalczyk–Hernández and the Applicant prepared and implemented the course. Since 2012 the Applicant is the coordinator (chief) of the course. The Applicant also co-authored a paper focused on intraocular lens, is running a project on measurements of contact lenses using atomic force and confocal microscopy in cooperation with Laboratory of Imaging Tissue Structure and Function in Nencki Instutite of Experimental Biology and Bionanostructures Laboratory CeNT III UW, and is developing his own work group in vision science.

c) research papers published before obtaining the PhD degree

The list includes only research papers published in scientific journals included on the list of the *Journal Citation Reports.*

[1] A. Przybyszewska, J. Pniewski, T. Szoplik, "Supervised classification of Łobez forest area in Landsat images," (1999) Optica Applicata **29(4),** 529—542.

[2] J. Pniewski, T. Szoplik, "Compression of grayscale images based on subband decomposition using morphological filters," (2000) Optica Applicata **30(2-3),** 336—347.

[3] J. Pniewski, A. Sagan, T. Szoplik, "Contrast control for grey-level deformation removal in images: an algorithm and a computer application," (2003) Computers & Geosciences **29(10),** 1241—1247.

d) research papers published after obtaining the PhD degree

The list includes only research papers published in scientific journals included on the list of the *Journal Citation Reports.* The list includes papers contained in the applicant's cycle of research papers related in scope and subject.

[1] T. J. Antosiewicz, W. M. Saj, J. Pniewski, T. Szoplik, "Optimization of optical transmittance of a layered metamaterial on active pairs of nanowires," (2006) Opt. Express **14(8),** 3389—3395.

[2] J. Pniewski, T. Szoplik, "Group front evolution of Gaussian beam refracted from a right- to left-handed medium," (2006) Opt. Express **14(18),** 8232—8239.

[3] W. M. Saj, T. J. Antosiewicz, J. Pniewski, T. Szoplik, "Energy transport in plasmon waveguides on chains of metal nanoplates," (2006) Opto-Electronics Review **14(3),** 167—262.

[4] P. Wróbel, J. Pniewski, T. J. Antosiewicz, T. Szoplik, "Focusing radially polarized light by a concentrically corrugated silver film without a hole," (2009) Physical Review Letters **102(18),** 183902.

[5] S. Mühlig, C. Rockstuhl, J. Pniewski, C.R. Simovski, S.A. Tretyakov, F. Lederer, (2010) Three-dimensional metamaterial nanotips, Physical Review B — Condensed Matter and Materials Physics **81(7),** 075317.

[6] P. Wróbel, T. J. Antosiewicz, J. Pniewski, T. Szoplik, "Single-layer metal nanolenses with tight foci in far-field," (2011) Applied Physics A: Materials Science and Processing **103(3),** 821—825.

[7] R. Buczynski, J. Pniewski, D. Pysz, R. Stepien, R. Kasztelanic, I. Kujawa, A. Filipkowski, A.J. Waddie, M. R. Taghizadeh, "Dispersion management in soft glass all-solid photonic crystal fibers," (2012) Opto-electronics Review **20(3),** 207—215.

[8] J. Pniewski, R. Kasztelanic, D. Pysz, R. Stępień, R. Buczyński, "Supercontinuum generation in all-solid photonic crystal fibers with a low index subwavelength inclusion in the core," (2013) Laser Physics **23(8),** 085104.

[9] M. Klimczak, B. Siwicki, P. Skibinski, D. Pysz, R. Stepien, A. Szolno, J. Pniewski, C. Radzewicz, R. Buczynski, "Mid-infrared supercontinuum generation in soft-glass suspended core photonic crystal fiber," (2014) Optical and Quantum Electronics **46(4),** 563—571.

[10] G. Stępniewski, J. Pniewski, M. Klimczak, T. Martynkien, D. Pysz, R. Stępień, I. Kujawa, K. Borzycki, R. Buczyński, "Broadband dispersion measurement of photonic crystal fibers with nanostructured core," (2015) Optical and Quantum Electronics **47(3),** 807—814.

[11] M. Sokołowski, J. Pniewski, R. Brygoła, M. Kowalczyk-Hernández, "Hybrid heptafocal intraocular lenses," (2015) Optica Applicata **45(3),** 285-298.

[12] J. Pniewski, T. Stefaniuk, G. Stepniewski, D. Pysz, T. Martynkien, R. Stepien, R. Buczynski, "Limits in development of photonic crystal fibers with a subwavelength inclusion in the core," (2015) Optical Materials Express **5(10),** 2366—2376. (Wyróżnienie Spotlight on optics.

[13] J. Pniewski, R. Kasztelanic, J. M. Nowosielski, A. Filipkowski, B. Piechal, A. J. Waddie, D. Pysz, I. Kujawa, R. Stepien, M. R. Taghizadeh, R. Buczynski, "Diffractive optics development using a modified stack-and-draw technique," (2016) Applied Optics **55(18),** 4939-4945.

[14] J. Pniewski, T. Stefaniuk, H. Le Van, V. C. Long, L. C. Van, R. Kasztelanic, G. Stępniewski, A. Ramaniuk, M. Trippenbach, R. Buczyński, "Dispersion engineering in nonlinear soft glass photonic crystal fibers infiltrated with liquids," (2016) Applied Optics **55(19),** 5033-5040.

[15] J. Pniewski, G. Stepniewski, R. Kasztelanic, B. Siwicki, D. Pierscinska, K. Pierscinski, D. Pysz, K. Borzycki, R. Stepien, M. Bugajski, R. Buczynski, "High numerical aperture large-core photonic crystal fiber for a broadband infrared transmission," (2016) Infrared Physics & Technology **79,** 10—16.

e) Bibliometric indicators

- Sum impact factor according to JCR and to the year of publishing: **34.916**
- Number of citations after Web of Science (WoS): **136**
- Number of citations excluding auto-citations after Web of Science: **120**
- Hirsch index after Web of Science: **5** (Scopus: 6)

As for 15.10.2016

Jacek Pniewski